UCRL-11088

University of California

Ernest O. Lawrence Radiation Laboratory

NEUTRON SPECTRA FROM HEAVY-ION BOMBARDMENT OF GOLD

Berkeley, California

DISCLAIMER

Research and Development

UCRL-11088
UC-34 Physics
TID-4500 (24th Ed.)

UNIVERSITY OF CALIFORNIA
Lawrence Radiation Laboratory
Berkeley, California

AEC Contract No. W-7405-eng-48

NEUTRON SPECTRA FROM HEAVY-ION BOMBARDMENT OF GOLD

William G. Simon

(Ph. D. Thesis)

October 21, 1963

Printed in USA. Price $2.00. Available from the
Office of Technical Services
U. S. Department of Commerce
Washington 25, D.C.

Contents

NEUTRON SPECTRA FROM HEAVY-ION BOMBARDMENT OF GOLD

William G. Simon

Lawrence Radiation Laboratory
University of California
Berkeley, California

October 21, 1963

ABSTRACT

Neutron yields from the bombardment of a Au target by 164- and 142-MeV O^{16} ions have been measured at angular intervals of 15 deg from 0 to 165 deg. Neutrons with energy from 0 to 12 MeV were detected by means of nuclear emulsions with use of the internal-radiator method. The 0-deg-yield measurements were extended to a neutron energy of 25 MeV by using a polyethylene radiator together with nuclear emulsions for neutron detection. The yields at 164 and 142 MeV are subtracted in order to obtain differential cross sections averaged over this energy interval, which are then transformed to the center-of-mass system. It is known that this reaction leads to fission in most cases, so that the problem of neutron-fission competition arises. The anisotropy coefficient, a, defined by the expression $W(\theta) = 1 + a \cos^2\theta$, is about 1 for 2-MeV neutrons and decreases rapidly with neutron energy. The distribution of neutrons is essentially isotropic above 6 MeV. This behavior disagrees with calculations of the angular distribution of neutrons from fission fragments, which are based on measured fragment angular distributions. It is concluded that some neutrons are emitted from the system before fission occurs. Calculations of the ratio of the neutron to fission width agree with this conclusion. The use of the internal-radiator method of neutron detection requires that the escape probability for protons from the emulsion layer be evaluated. Measurements of the multiple scattering of stopping protons, which were used in evaluating this probability, are reported in Appendix II. These measurements are in agreement with theory.

I. INTRODUCTION

There are two differences between reactions induced by heavy ions ($A \gtrsim 4$) and those induced by light particles, which account to a large extent for the interest in heavy-ion reactions. First, the angular momentum can be very large. In this experiment, where Au^{197} nuclei are bombarded by O^{16} ions of approx 152 MeV, angular momenta as high as 90 $\hbar$ are involved. Second, compound nuclei with very high excitation energies (> 100 MeV) and with relatively definite initial conditions may be formed. If light particles with this much energy are used for bombardment, an initial "cascade" takes place before the energy, initially concentrated on one or a few nucleons, becomes uniformly distributed among the nucleons of the compound system. Several nucleons may be emitted during this cascade stage, thus complicating the interpretation of the reaction.

Throughout the discussion, the concept of a compound nucleus is applied. The assumption is made that a nuclear reaction can be divided into two independent stages: (a) the formation of the compound system, and (b) the decay stage. The mode of decay is assumed to depend only on the energy, angular momentum, and parity of the compound system. These assumptions hold only approximately for the case considered here. Direct-type interactions such as α stripping contribute to the total reaction. Furthermore, it is possible for particles to be emitted from the system before the energy is shared among all the nuclei; i.e., in a period of time shorter than the relaxation time for the nucleus. Certain types of reaction products may be interpreted in terms of the compound-nucleus picture, whereas others may not. Alpha particles from this reaction are peaked strongly forward,[1] which indicates a direct component of the α spectra about twice as large as the evaporation component. For neutrons, measured in this work, there is no evidence of forward peaking.

A compound nucleus may decay in many different ways. Let $P_\nu(E, U)dE$ be the probability per unit time that a nucleus with excitation energy U emits a particle of type ν with energy between E and E + dE. An application of the principle of detailed balance leads to the expression[2]

$$P_\nu(E, U)dE = \frac{(2S_\nu + 1)\mu_\nu E\sigma_\nu\rho_\nu(U - E_s - E)dE}{\pi^2\hbar^3\rho_c(U)} ,$$

where $(2S_\nu + 1)$ is a statistical factor,

S_ν is the spin of ν,

μ_ν is the reduced mass,

σ_ν is the cross section for the time-reversed process,

$\rho_\nu(U-E_s-E)$ is the density of states of the residual nucleus, the argument is its excitation energy, and

E_s is the energy necessary to separate the evaporated particle from the compound nucleus.

The density of states of the initial nucleus is symbolized by $\rho_c(U)$. This basic equation of the statistical model requires a knowledge of the time-reversed cross section σ_ν, and of the level density of the compound nucleus. Here, σ_ν is not measurable because it refers to reactions of the decay product on excited nuclei. Neutron cross sections are not expected to vary appreciably with the excitation energy of the nucleus so that the geometrical cross section $\pi r_0^2 A^{2/3}$ is satisfactory. The level density is generally assumed to be of the form

$$\rho(U) \propto e^{2(aU)^{1/2}} ,$$

where a is a constant. If angular momentum is explicitly included, this level-density formula is altered, as discussed in Section III.

For heavy nuclei, the emission of charged particles is so inhibited by the Coulomb barrier that neutron emission dominates the de-excitation process. For the reactions studied in this experiment, fission occurs about 80% of the time,[3] and, of course, an interpretation of the neutron spectra cannot be made without examining the effects of fission.

Measurements of the charged-particle spectra for this reaction have been made by Britt and Quinton[1] and by Reames.[4] The angular distribution of the fission fragments has been measured by Viola,[5] and the angular and energy distributions have been measured by Britt and Quinton.[3] Yield-mass and yield-charge distributions for the neighboring reaction C^{12} + Au have been studied by Blann,[6] and by Thomas et al.[7]

Measurements of the total neutron yields for the similar reactions C^{12} + Au and Ne^{20} + Au have been made by Hubbard et al.[8] The energy and angular distributions of neutrons have been made by Breck,[9] who used surface-barrier counters for detection of the recoil-proton energy spectrum, and differentiated this to obtain the neutron spectrum.

II. EXPERIMENTAL PROCEDURE

A. Emulsion Exposure

1. Beam Geometry

The experimental arrangement is shown in Fig. 1. It is designed to obtain a well-collimated beam of small profile at the target and, at the same time to do everything possible to minimize the neutron background that originates when the beam hits matter other than the target. The O^{16} ions leave the accelerator with an energy of 166 MeV. A 4-in. quadrupole lens focuses the beam at the target. The object for this lens is a 0.5-in. -diam collimator placed near the Hilac exit. A 1-in. -diam carbon collimator placed 21 in. in front of the quadrupole lens eliminated all beam particles that would scatter from the beam pipe at a point closer to the target. This collimator was located 175 in. from the emulsion detectors, so that the solid-angle factor for neutrons originating in the collimator was very small (the target-to-emulsion distance was 8 in.). To further reduce the background from this slit, about 3.5 ft of paraffin shielding was placed between it and the emulsion detectors.

In order to tune the beam, we placed a quartz crystal with a thin aluminum foil on the beam side in the target position and viewed it from the downbeam side with a television camera. The foil and crystal formed the back of a Faraday cup, so that beam measurements could be taken while we were viewing the crystal. The beam diameter measured in this way was $\leq 1/4$ in. The beam pattern at the target was observed several times between runs, and no changes were detected. If the quadrupole lens is adjusted to focus a parallel beam, the position of the beam at the target is insensitive to the position of the beam in the object diaphragm; thus, any wandering of the beam leaving the accelerator would not alter the position of the beam at the target.

The beam was measured by using a Faraday cup. This cup was a tube 2-3/4 in. in diam and 15 in. long with 1/32-in. walls, insulated from the beam pipe by Teflon insulators specially shaped to reduce

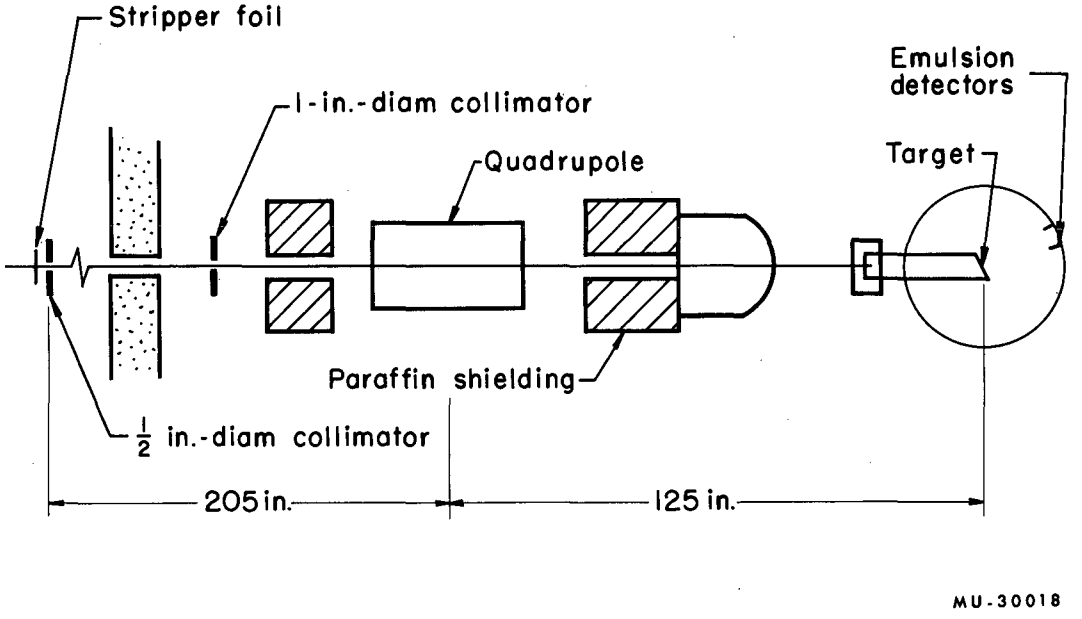

Fig. 1. Experimental arrangement for neutron detection with emulsion used as both detector and radiator.

leakage current. The rear end of the tube was cut at 60 deg to its axis, and a brass ring was soldered on to support the target. The thick Au target (132.5 mg/cm^2) formed the back of the Faraday cup.

2. Neutron Detection

We detected neutrons by means of nuclear emulsions, using the internal recoil method. The 1×3-in. glass-backed emulsions were placed a distance of 8 in. from the target at 15-deg intervals from 0 to 165 deg. The plane of the emulsion contained the radial line from the target, and the 3-in. edge was perpendicular to this line. The 1/32-in. brass front covers of the cameras stopped most of the charged particles from the target. The emulsions used were 600-μ Ilford type K-2 and K-5. In some cases the plates were exposed in pairs with the emulsion faces together. This greatly reduced the flux of charged particles entering the surface of the emulsion, and thus increased the ease of scanning.

3. Arrangement of External-Radiator Experiment

The experimental arrangement for measuring the neutron yields by using an external radiator is shown in Fig. 2. The beam geometry was similar to that in the internal-radiator setup except that the quadrupole-to-target distance was shorter. The beam was measured by using a Faraday cup. The thick Au target, which formed the back of the Faraday cup, was backed by a 3/32-in. thick piece of lead, which stopped charged particles originating in the target. A polyethylene radiator was placed 14 in. from the target in the forward direction. Nuclear emulsions located 6 in. from the radiator at angles from 20 to 30 deg to the beam direction were used to detect the recoil protons. The polyethylene shield in Fig. 2 protected the emulsions from neutrons coming directly from the target, which would blacken the emulsions if not attenuated.

All protons entering the emulsion surface are assumed to originate from n-p collisions within the polyethylene radiator. Those not originating in this way constitute background. The amount of background

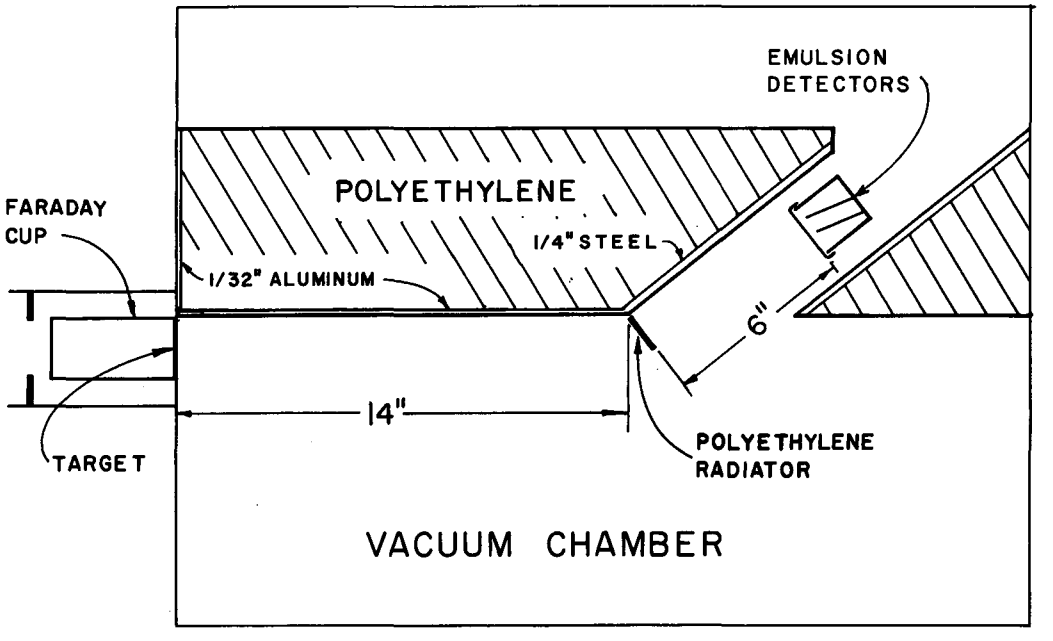

Fig. 2. Experimental arrangement for neutron detection with the use of an external polyethylene radiator.

present could thus be estimated by replacing the polyethylene radiator by a dummy radiator containing no hydrogen. For this purpose, a thin carbon sheet, containing the same number of C atoms per cm^2 as the polyethylene radiator was used. This did not exactly simulate the polyethylene in that it was less effective in stopping protons passing through it. However, this effect is not large because most of the background protons entering the emulsion surface probably originate in the walls of the vacuum chamber, and the total correction is only 9.4%.

The target-radiator-detector system used is a compromise between the intensity problem encountered with too "tight" a geometry and the problems of inaccuracy arising from too open a geometry.

B. Beam Energy

The Hilac accelerates ions to a velocity corresponding to 10.4 MeV per nucleon. This velocity is fixed by the length of the drift tubes in the accelerator cavities and cannot be altered (except that half-velocity particles can be obtained). The charge of O^{16} ions exiting the accelerator is generally six, but may be five or seven, or some combination of these. Thus, for reliable beam measurements, it is best to use a stripper foil that reduces the beam to a known charge.

Runs were made at 164 MeV and at 142 MeV. For the full-energy runs, a 0.1-mil Al stripper foil was used; for the 142-MeV runs, a 1.7-mil degrader-and-stripper foil was used. The beam energies were measured by observing the particle ranges in nuclear emulsion. Ilford type C-2 glass-backed emulsions were exposed to the beam with the emulsion surface at an angle of 5 deg to the beam direction. The particle ranges were measured under high magnification with the use of a calibrated eyepiece reticle. The range-energy relation of Heckman et al.[10] was used to determine the energy of the particles. The following corrections were applied to the measured ranges: (a) Emulsion density corrections were made according to Barkas.[11] The emulsions were exposed in vacuum so that the volume through which the ions pass, being near the surface, was assumed to be "dry" (density 4.05). (b) One mean grain diameter (0.35 μ) is subtracted to correct for the extension of the first and last grain of the track.[11] The results of these

energy measurements are given in Table I. Comparison with the measurements by Northcliffe[12] are made. The two lowest-energy runs were not used in this experiment. The measured energy straggle includes the effects of range straggling in the emulsion (≈ 1%).

Table I. Comparison of measured and calculated beam energies.

Nominal degrader thickness (mils)	Measured thickness (mg/cm^2)	Calculated energy[a] (MeV)	Measured energy (MeV)	Energy straggle (MeV)
0.1	0.70	---	164.0±0.6	2.5
1.7	12.22	141.0	141.9±0.7	2.6
3.2	22.22	115.3	115.6±0.5	2.5
4.25	28.22	97.7	97.1±0.6	2.7

[a] These values were obtained with use of the range measurements for heavy ions in aluminum by Northcliffe.

C. Shrinkage Factor of the Emulsions

Emulsion shrinks during processing. The fact that the pellicle is mounted on glass constrains the shrinkage to the z direction. The shrinkage factor, which is the ratio of the thickness of the unprocessed to the processed emulsion, was measured in the following way: The unprocessed emulsion contains some naturally radioactive substances. Some decays occur during the storage time of the emulsion and leave identifiable tracks. The range R of these tracks in emulsion after processing satisfies the relation

$$R^2 = \ell^2 + s^2 z^2,$$

where ℓ is the projection of the range in the plane of the emulsion,

s is the shrinkage factor,

and z is the projection of the range on the normal to the emulsion.

Thus a plot of ℓ^2 vs z^2 gives a slope equal to s^2. The most useful decays are from Th C', which has an unusually large Q value of 8.776 MeV. These decays can easily be identified because the α range exceeds that of any other common decay by 9 μ. This extra length also yields more accurate measurements. Ra C' events were also found to be useful for these measurements.

If the emulsions are processed shortly after manufacture, it may be difficult to locate a sufficient number of events.

Figure 3 is a plot of ℓ^2 vs z^2 for one plate; the line is a least-squares fit that gives a slope corresponding to $s = 2.46 \pm 0.06$. This method has been suggested by Barkas,[13] but apparently had never been applied in practice.

D. Emulsion Scanning and Data Analysis

1. Internal Radiator Method

In the internal-radiator method, the analysis is based on neutron-proton collisions that occur in the emulsion. If the direction of the incoming neutron is known, then its energy is given nonrelativistically by

$$E_n = E_p(R)/\cos^2\theta, \qquad (1)$$

where R is the measured range, θ is the angle between the neutron and proton directions, and $E_p(R)$ is the energy of the recoil proton. A measurement of R and θ completely specifies the energy of the neutron. An analysis based upon the measurement of both R and θ and a subsequent calculation according to Eq. (1), is called the individual-track method. The traditional method of measurement and analysis, called the average-angle method, is to choose a small cone of acceptance in the forward direction and reject all tracks outside this cone.[14] The energy of the neutron is taken to be a value that represents an average for all neutrons producing a proton with range equal to that of the measured proton. The main disadvantage to this method is that the small cone of acceptance results in a large error in determining which tracks lie within the cone; its main advantage is the ease of analysis. We used a coordinate readout microscope together with

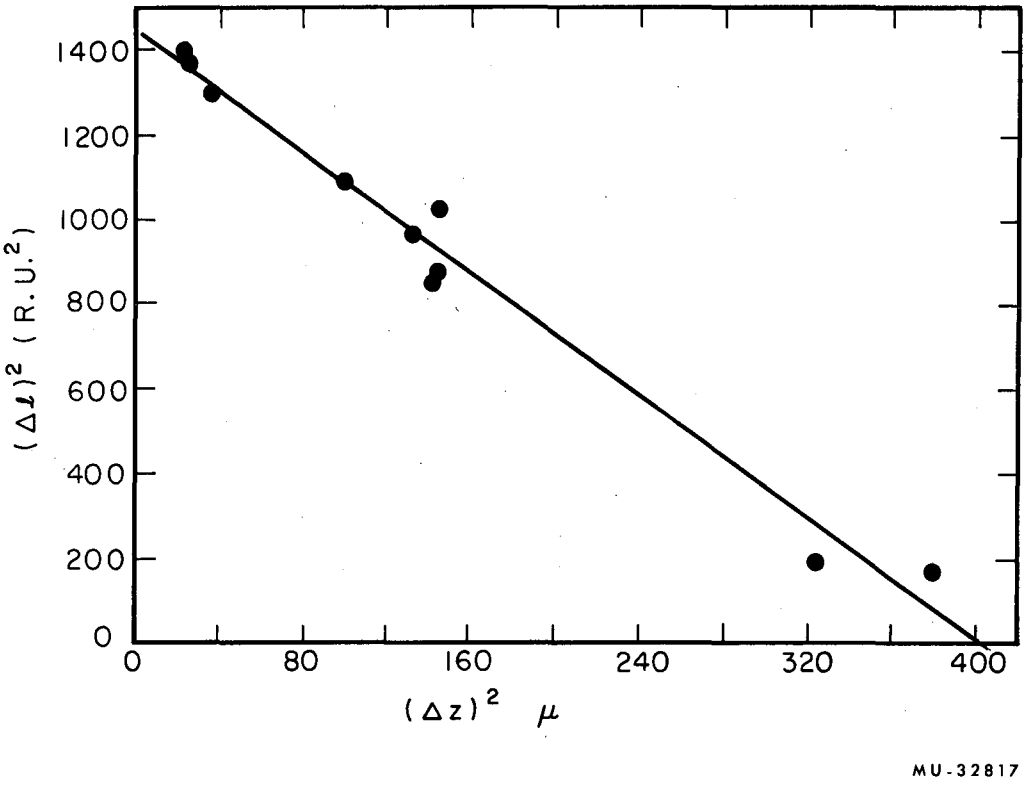

Fig. 3. Plot for the determination of emulsion-shrinkage factor. The projected range squared, ℓ^2, in units of the eyepiece reticle (1 R. V. = 1.306 μ) is plotted against the square of the z extent of the track. The line shown is a least-squares fit, which gives a shrinkage factor equal to 2.46 ± 0.06.

digital computers for analysis. This allowed us to use the individual-track method without spending an unduly large amount of time in measurement and analysis. The fractional uncertainty of the neutron energy caused by an error in angular measurement $d\theta$ is, according to Eq. (1),

$$\frac{dE_n}{E_n} = 2 \tan\theta d\theta.$$

Because the error increases without limit for large θ, it is necessary to choose an acceptance cone and use only protons with $\theta < \theta_{max}$. The neutron flux through the emulsion is given by

$$F(E_n) = \frac{n_c}{dE_n \, n_p \, \sigma_{np}(E_n) \, C[1-P(E_n, \theta_{max})]} , \quad (2)$$

where n_p is the number of protons per cm^3 in the emulsion,

$F(E_n)dE_n$ is the number of neutrons/cm^2 traversing the emulsion with energy between E_n and E_n+dE_n,

n_c is the number of proton recoils per cm^3 of emulsion that correspond to neutron energies between E_n and E_n+dE_n and which have $\theta < \theta_{max}$,

$\sigma_{np}(E)$ is the total n-p cross section for neutrons of energy E_n,

C is the fraction of all recoil protons that have $\theta < \theta_{max}$,

and $P(E_n, \theta_{max})$ is the probability that a proton produced by a neutron of energy E_n and lying in the cone $\theta < \theta_{max}$ leaves the emulsion. This quantity is discussed in Appendix II.

The factor C can be easily determined if the scattering is isotropic in the center-of-mass system (this assumption is accurate for neutron energies $\leq$ 14 MeV). Then the c. m. distribution $P(\theta^*)$ is

$$P(\theta^*)d\theta^* = \frac{\sin\theta^*}{2} d\theta^*,$$

where θ^* is the scattering angle in the center-of-mass system. The laboratory-system distribution is then given by

$$P(\theta)d\theta = P(\theta^*) \frac{d\theta^*}{d\theta} d\theta .$$

With $\theta^* = 2\theta$, we have

$$P(\theta)d\theta = 2\sin\theta\cos\theta d\theta$$

and

$$P(\theta < \theta_{max}) = \int_0^{\theta_{max}} 2\sin\theta\cos\theta d\theta = \sin^2\theta_{max};$$

hence, $C = \sin^2\theta_{max}$.

For a center-of-mass distribution of the form $\frac{d\sigma}{d\Omega} \propto 1 + 2A\cos^2\theta^*$ (a P wave contribution to the scattering has been added;), the corresponding result is

$$1/C = \frac{1 + 2/3A}{\sin^2\theta_{max} + \frac{A}{3}(1 - \cos^3\theta_{max})} .$$

This is the form used in this analysis, with values of A given by Gammel.[15] The neutron yield, $Y(E, E_n, \theta)$, for an incoming beam energy E at laboratory-system angle θ is defined as the flux per unit solid angle per unit neutron energy divided by the total number of incoming particles; thus

$$Y(E, E_n, \theta) = \frac{F(E_n)}{r^2 N} , \qquad (3)$$

where $F(E_n)$ is measured for a beam energy E at laboratory-system angle θ. Here, r is the target-to-detector distance, and N is the total number of incident beam particles. If we know these yields at two energies E_1 and E_2, we may calculate an average cross section over the region $E_1 < E < E_2$. This is given by

$$\frac{d^2\sigma}{d\Omega dE_n} = \frac{Y(E_2, E_n, \theta) - Y(E_1, E_n, \theta)}{[R(E_2) - R(E_1)]\frac{A_0}{A}} , \qquad (4)$$

where $R(E)$ is the particle range in the target material in g/cm^2, A_0 is Avogadro's number, and A is the atomic mass of the target nucleus.

a. Emulsion scanning.

Scanning was done with the use of a digital coordinate readout microscope the output from which is recorded on IBM cards. Three

analog-to-digital converters, connected to the three coordinate screws of the microscope, transform their angular positions to digital electrical form. This binary information is then converted to decimal form and fed to an IBM card punch. The coordinates are punched in fixed-point decimal form in units of microns for the x and y coordinates and in units of 0.6 micron for the z coordinate. The scanning procedure is as follows: The scanner begins by recording the z coordinates at the top and bottom of the emulsion at some standard point. This measurement relates the thickness of the emulsion at the time of scanning to that at the time shrinkage factors were measured. Next the "fiducial point" of the emulsion is recorded. This is the point at which the target-to-emulsion line intersects the front edge of the emulsion normally (Fig. 4). Track scanning begins at a point 2 mm from the front edge of the emulsion to avoid the excessive edge distortions.

To determine the volume of emulsion scanned, the scanning proceeds by "fields of view," which are sequentially numbered and recorded on the IBM cards. A field of view consists of a volume of emulsion extending from the top to the bottom of the emulsion and defined in the xy plane by lines on an eyepiece reticle. Each proton track that originates in the field of view is measured. Thus, after a track is measured, the x and y coordinates must be returned to their original positions. This process was greatly facilitated by use of a ball-bearing device in the lead-screw control knob and readout dial assembly, which allows the scanner to return readily to the original center coordinates of the field of view. This apparatus is shown in Fig. 5.

The position coordinates of a track are recorded at its origin, at a second point chosen to give the best measure of the orientation of the track, and at as many subsequent points as are necessary to determine the range.

b. Track analysis

The emulsion-target geometry is shown in Fig. 4. We define the following quantities: x_1, y_1, z_1 and x_2, y_2, z_2 are the coordinates of the beginning of the proton track and the second point measured, referred to the emulsion axes, which are aligned with the movement of the microscope stage;

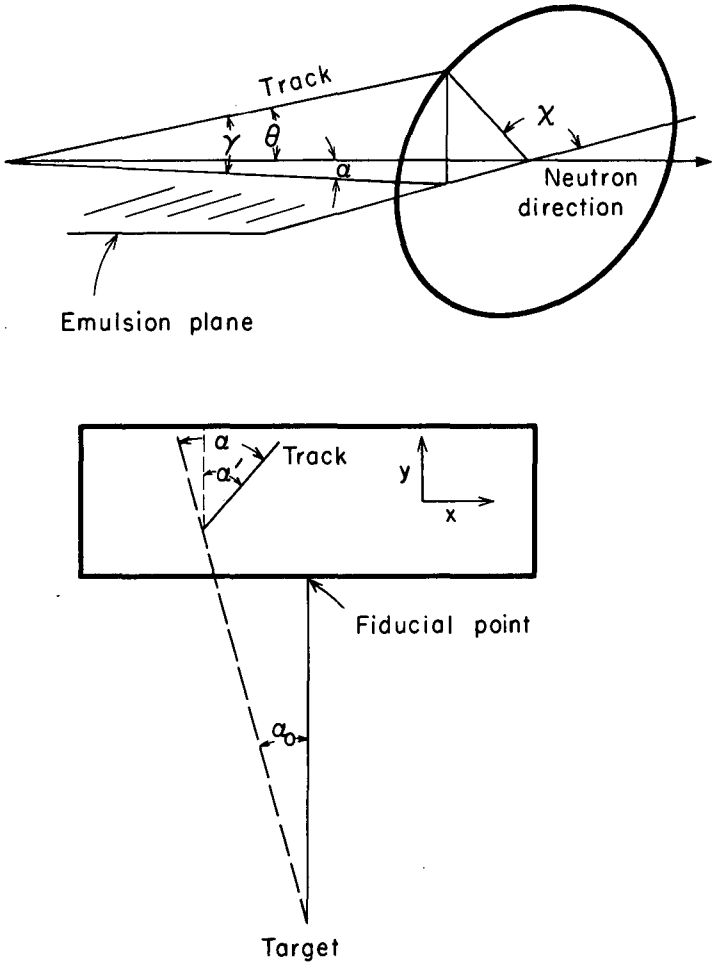

Fig. 4. Two drawings illustrating track and emulsion geometry; see text.

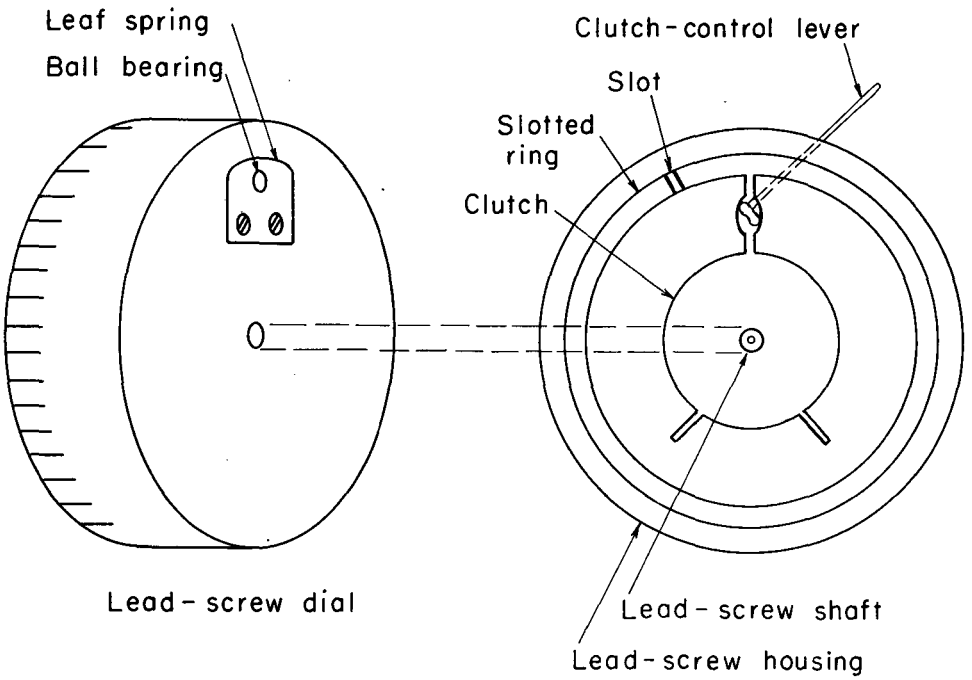

Fig. 5. Apparatus, designed by James C. Hodges, to return microscope stage to a predetermined position. For complete discussion of microscope stages, the reader should refer to the report of Hodges.[31] The parts of the lead-screw dial are shown separated for viewing. A ring with a radial slot in it is recessed into the lead-screw housing. A clutch, consisting of a broken ring with an eccentric to spread it, locks the ring when engaged. When the clutch is not engaged, the ring rotates freely. A ball bearing is attached to a leaf spring that is fixed on the lead-screw dial. When the apparatus is in its assembled position, the spring forces the bearing against the slotted ring. The principle of operation is as follows: With the clutch disengaged and the ball bearing in the slot, the slotted ring rotates freely with the lead-screw dial. The scanner engages the clutch when the lead screw is in the initial position, A. Now when the lead screw is turned, the ball bearing leaves the slot and rides along the ring without rotating it. When the lead screw is returned to position A (or, this position plus an integral number of turns), the ball bearing snaps into the slot in the ring, thus indicating to the scanner that the microscope stage is in its original position.

α' is the angle between the projection of the proton track in the xy plane and the y motion of the microscope stage;

α_0 is the angle between the neutron direction (which is in the emulsion plane) and the y motion of the microscope stage;

d is the target-to-fiducial distance;

γ is the angle between the track direction and the emulsion plane (dip angle);

and x_f, y_f are the coordinates of the fiducial point.

Then from Fig. 4, we see that

$$\cos^2\theta = \cos^2(\alpha' - \alpha_0)\cos^2\gamma = [(\cos\alpha'\cos\alpha_0 + \sin\alpha'\sin\alpha_0)\cos\gamma]^2.$$

In terms of measured quantities, we have

$$\cos\alpha' = \frac{y_2 - y_1}{[(y_2 - y_1)^2 + (x_2 - x_1)^2]^{1/2}};\quad \cos\alpha_0 = \frac{d + y_1 - y_f}{[(d+y_1-y_f)^2 + (x_1 - x_f)^2]^{1/2}};$$

$$\cos\gamma = \frac{[(y_2 - y_1)^2 + (x_2 - x_1)^2]^{1/2}}{[(y_2 - y_1)^2+(x_2-x_1)^2+S^2(z_2-z_1)^2]^{1/2}};$$

and $$\sin\alpha_0 = \frac{(x_1 - x_f)}{[(d+y_1 - y_f)^2 + (x_1 - x_f)^2]^{1/2}}.$$

Putting these into the above equation, we have

$$\cos^2\theta = \frac{[(y_2 - y_1)(d + y_1 - y_f) + (x_1 - x_f)(x_2 - x_1)]^2}{[(d+y_1 - y_f)^2 + (x_1 - x_f)^2(y_2 - y_1)^2 + (x_2 - x_1)^2 + S^2(z_2 - z_1)^2]}. \tag{5}$$

The angle α_0 never becomes larger than approx 1/8 radian, and hence we can neglect quantities of order α_0^2 with an error of less than 1 in 64. Thus we neglect $(x_1 - x_f)^2$ compared with $(d+y_1 - y_f)^2$. Furthermore, $(y_1 - y_f)/d$ never exceeds 1/16, so that $(y_1 - y_f)(x_1 - x_f)/d^2$ can be neglected. Making these approximations, we get, after rearranging

$$\cos^2\theta = \frac{[\,|y_2 - y_1| + (x_2 - x_1)(x_1 - x_f)/d\,]^2}{R^2} \quad ,$$

where R is the range of the first measured segment of track, i.e.,

$$R^2 = (x_2 - x_1)^2 + (y_2 - y_1)^2 + S^2(z_2 - z_1)^2 .$$

These equations together with the total proton range allow us to determine the energy of the neutron as well as $\cos^2\theta$. We also wish to find the azimuthal angle ψ. This is found from the two relations

$$\sin\psi = \frac{\sin\gamma}{\sin\theta} = \frac{S(z_2 - z_1)}{R(1-\cos^2\theta)^{1/2}}$$

and

$$\cos\psi = \frac{x_2 - x_1}{|y_2 - y_1|} - \frac{x_1 - x_f}{d} \quad .$$

The signs of $\sin\psi$ and $\cos\psi$ determine the quadrant of ψ, so that the above two equations completely determine ψ. The data cards were processed by an IBM 650 computer. The computer was programmed to tabulate the following information:

(1) For each track the values of E_n, $\cos^2\theta$, and ψ.

(2) Tables of the number of tracks recorded in each 10-deg interval of ψ with E_n in each of three chosen intervals, and the ψ distribution of all the tracks.

(3) Tables of the number of tracks recorded in each 0.01 interval of $\cos^2\theta$ with E_n in each of three chosen intervals, and the $\cos^2\theta$ distribution of all the tracks.

(4) Tables of the number of tracks recorded with E_n in 0.1-MeV intervals from 0 to 10 MeV, and 1-MeV intervals above 10 MeV. Also the neutron yield, calculated according to Eq. (3) and its statistical error. These calculations were tabulated for each two chosen cones of acceptance, defined by θ_{1max} and θ_{2max}.

2. External Radiator Method

In this case the proton recoils from the radiator enter the emulsion surface with dip angles of about 15 deg. The method of scanning is simply to measure the range of each track that enters the emulsion surface within a given area A. The relation between the number of tracks counted and the neutron flux at the radiator is derived in Appendix I [Eq. (13)]. The neutron yield is then given by

$$\frac{d^2Y}{d\Omega dE} = \frac{d^2N_0}{d\Omega dE} \times \frac{1}{r^2 N} ,$$

where $d^2N_0/d\Omega dE$ is the neutron flux at the radiator as given by Eq. (13). Here, r^2 is the target-to-radiator distance, and N is the total number of incident beam ions.

3. Background Analysis

With the individual-track method of analysis one can compare the observed angular distributions of the proton tracks with that required by the known n-p differential cross section. Deviations from the required distributions are indications of background. The proton distribution with respect to both $\cos^2\theta$ and ψ must be uniform. As before, θ and ψ are the polar and azimuthal angles between the proton direction and the direction to the target. An analysis of these distributions showed no systematic deviations from uniformity other than those imposed by the finite mesh size of the coordinate readout. A still more sensitive test is the following: All recoil protons must be going away from the target. For protons with energy greater than 2 MeV, the direction of motion can be visually determined and this test applied. This test is especially sensitive for emulsion plates located at angles near 180 deg with respect to the beam direction. Here the neutron flux from the target is smallest, and also the background is expected to be coming from the direction of the accelerator, which is in the direction opposite to the target. Thus, for these emulsion plates the background is expected to be going predominantly towards the target and is therefore easily detected. It is estimated by this method that the background flux is less than 3% of the total neutron flux.

4. The Center-of-Mass Transformation

The yields at each lab angle were least-square fitted to the form

$$Y(E) = A E^{B} \exp(CE + DE^{2}),$$

where E is the neutron energy. This form was suggested by the Weisskopf, Maxwell, and Le Couteur distributions discussed in later sections. It includes these three distributions. It gives reasonable values of χ^2. This form is meant to be used only as an interpolation formula, so that the center-of-mass transformation program described below could be carried out. The c. m. transformations were then done in the following way: First a c. m. energy is chosen arbitrarily. Then for each laboratory-system angle, the corresponding laboratory-system energy and c. m. angle were found. The laboratory-system cross section is then determined from Eq. (4) and transformed to the c. m. system. The laboratory-system energy corresponding to c. m. energy E^* is

$$E = \left[\tau_{cn}^{1/2} \cos\theta + (\tau_{cn} \cos^2\theta + E^* - \tau_{cn})^{1/2} \right]^2 ,$$

where τ_{cn} is the laboratory-system kinetic energy of the compound system divided by its mass in units of the neutron mass. With this equation and the relations,

$$\sin\theta^* = \left(\frac{E}{E^*} \right)^{1/2} \sin\theta$$

and

$$\sigma_{c.m.}(E^*, \theta^*) = \left(\frac{E^*}{E} \right)^{1/2} \sigma(E, \theta) , \qquad (6)$$

one can make the transformation. The value of τ_{cn} used is an average for beam energies between 142 and 164 MeV computed from

$$\left\langle \tau_{cn}^{1/2} \right\rangle = \int_{E=142}^{164} \tau_{cn}^{1/2}(E)\, \sigma_{cn}(E)\, F(E)\, \frac{dR}{dE}\, dE ,$$

where σ_{cn} is the cross section for compound-nucleus formation, $F(E)$ is the average number of neutrons emitted, and $R(E)$ is the range of an

oxygen ion in Au. Values of σ_{cn} used were calculated by Thomas.[21] The value $F(E) = 9 + E-142/11$ was used.[6,8]

5. Systematic Errors that Affect the Normalization

The following errors were considered for the estimation of the overall error in normalization:

a. Target-to-emulsion distance: The maximum error in centering the beam is about 1/8-in.; this results in an error of 3%.

b. Beam integration: Comparison of beam measurements by a Faraday cup with Rutherford scattering by Gilmore[16] under similar circumstances indicate that the Faraday-cup readings are reliable to within about 4%.

c. Shrinkage factor: One effect of this error is to change the size of the cone of acceptance. To first order in small quantities, this affects the yields by the same factor as the error in the shrinkage factor (≈2-1/2%). The other effect of this error is to change the estimate of the volume of emulsion scanned. This error is in the same direction as the cone error. Hence the total effect on the yield is approx 5%.

d. Hydrogen density of emulsion: This error is estimated to be about 2%.

e. Errors in escape probability: These are discussed in Appendix II. The errors are small and are neglected.

f. The n-p cross sections: These are very well measured. The errors in this cross section are neglected.

g. Background: This is discussed in Section II. D; the value of this error is approx 2%.

It is assumed that the above errors add randomly. The resulting error in the normalization of the yields is then given by the square root of the sum of the squared errors, as can be seen from Eqs. (2) and (3), which involve the above quantities as factors. The resulting normalization error of the yield is approx 7.8%.

The cross section is given by Eq. (4),

$$\sigma = \frac{Y(164\ \text{MeV}) - Y(142\ \text{MeV})}{[R(164) - R(142)]\frac{A}{A_0}} .$$

The error in σ is then

$$\frac{\delta\sigma}{\sigma} = \left(\left\{ \frac{[\delta Y(164)^2 + \delta Y(142)^2]^{1/2}}{[Y(164) - Y(142)]} \right\}^2 + \left\{ \frac{[\delta R(164)^2 + \delta R(142)^2]^{1/2}}{[R(164) - R(142)]} \right\}^2 \right)^{1/2}.$$

The yields at 142 MeV are about 1/2 those at 164 MeV. Replacing 1/2 Y(164) = Y(142), we have

$$\frac{\delta\sigma}{\sigma} = \left\{ \frac{\left[\frac{\delta Y(164)}{Y(164)}\right]^2 + \left(\frac{1}{4}\right)\left[\frac{\delta Y(142)}{Y(142)}\right]^2}{\left(\frac{1}{4}\right)} + \left[\frac{\delta R(164)^2 + \delta R(142)^2}{[R(164) - R(142)]^2}\right] \right\}^{1/2}.$$

The second term under the radical is negligible compared with the first. Then our final estimate in the normalization error is

$$\frac{\delta\sigma}{\sigma} = 17.5\%.$$

III. RESULTS AND DISCUSSION

A. Experimental Results

Figures 6 through 12 show the measured yields. Figure 6 shows a comparison of yields obtained by external and internal radiator methods. The normalization between the two methods is good. The errors shown are statistical errors in the number of tracks counted. The main results of these measurements are illustrated by Fig. 13, which shows the angular distributions of neutrons in the center-of-mass system, and by Fig. 14, which displays the energy dependence of the neutron spectrum in the center-of-mass system. The curves shown in Fig. 13 are least-square fits to the form $\sigma(\theta^*) = \sigma(90\text{ deg})(1 + a\cos^2\theta^*)$. The cross section averaged over angle is then $\sigma(90\text{ deg})(1 + a/3)$. A summary of values of $\sigma(90\text{ deg})$, a, and the cross section averaged over angle is given in Table II.

Table II. Values of the cross section at 90 deg, the anisotropy, and the cross section averaged over the angle for various values of the neutron energy E.

E	σ (90 deg) (mb/MeV-sr)	a	Average cross section $\sigma_a = \sigma(90\text{ deg}) + a/3$
1.5	183 ± 39	1.05 ± 0.32	247
2	176 ± 37	0.81 ± 0.32	224
4	119 ± 14	0.159 ± 0.19	125
6	53.8 ± 4.5	0.047 ± 0.145	55
8	21.9 ± 2.1	0.099 ± 0.158	22.7

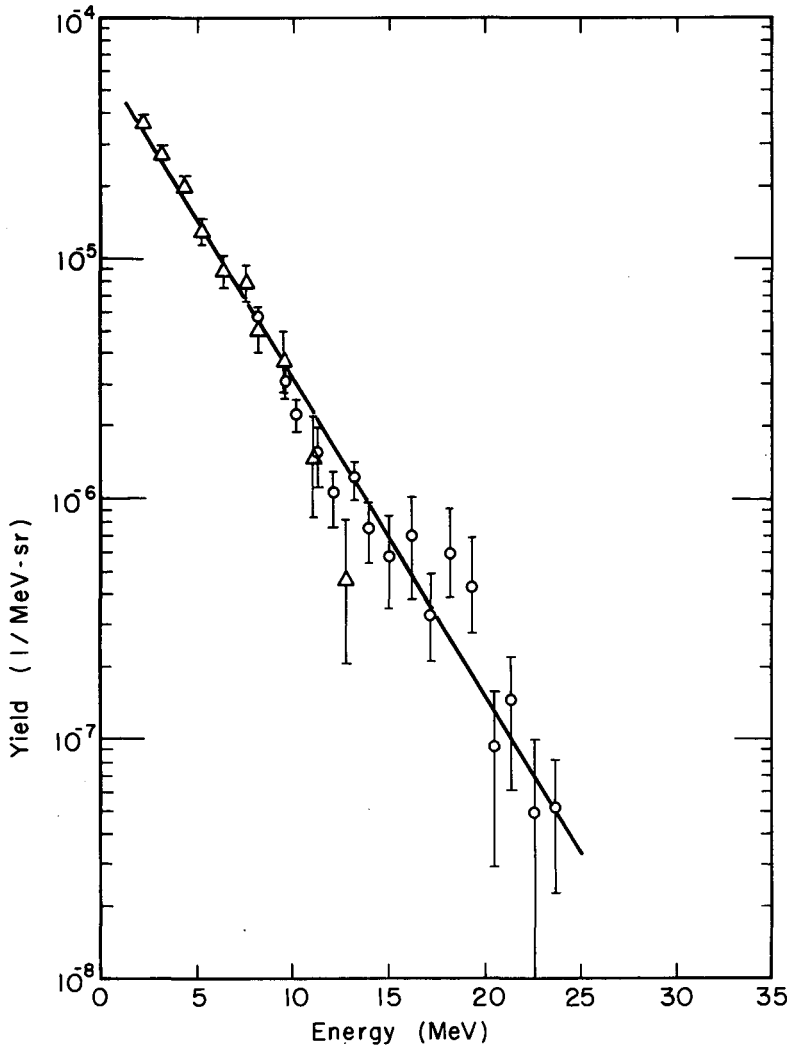

Fig. 6. Neutron yield in the laboratory system at 0 deg for 164-MeV O^{16} ions on a thick Au target. Triangles and circles designate points obtained with the use of internal and external radiator methods.

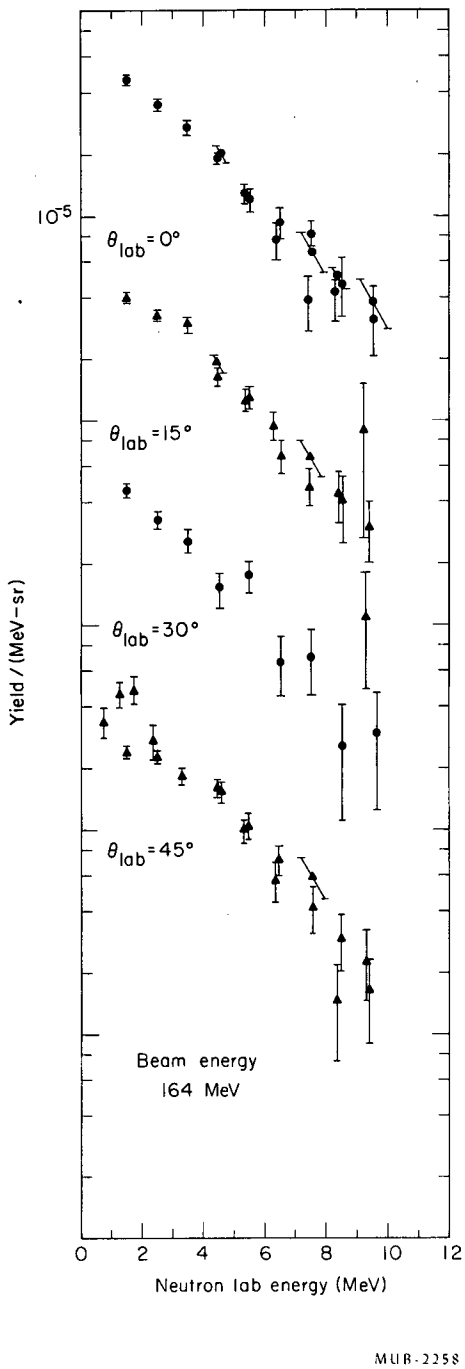

Fig. 7. Experimental results: The neutron yields are shown as a function of laboratory-system energy for laboratory-system angles shown. The absolute yields are indicated for the uppermost curve. Successive curves are displaced, each by one order of magnitude.

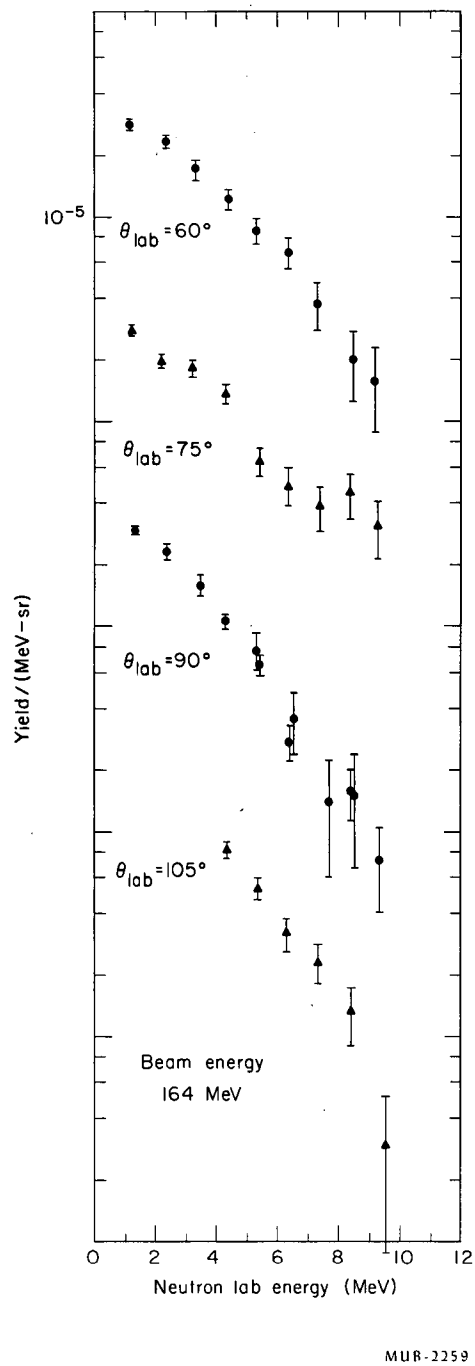

Fig. 8. Experimental results: The neutron yields are shown as a function of laboratory-system energy for laboratory-system angles shown. The absolute yields are indicated for the uppermost curve. Successive curves are displaced, each by one order of magnitude.

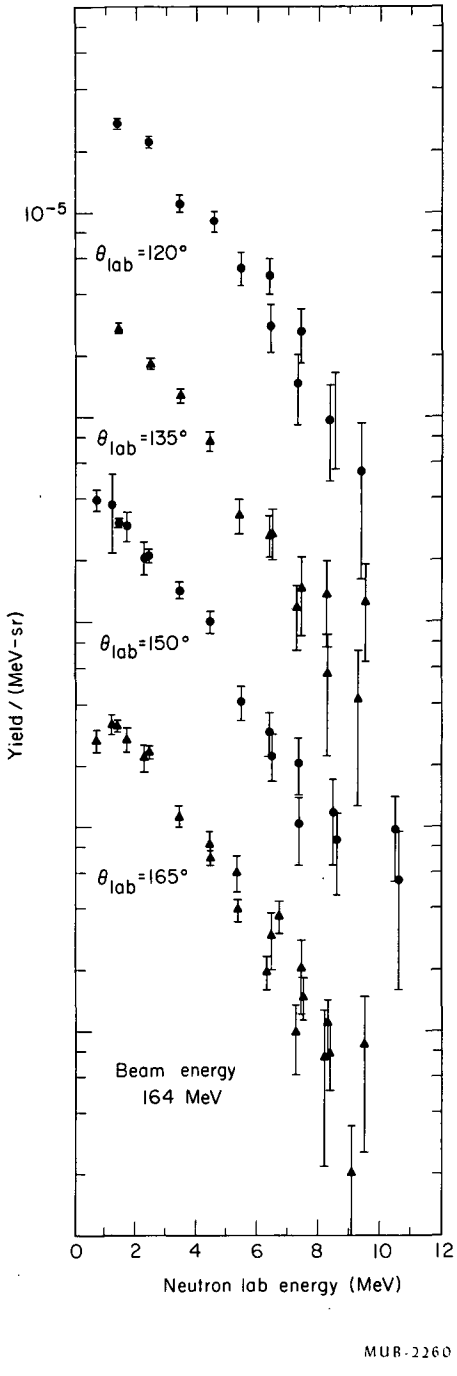

Fig. 9. Experimental results: The neutron yields are shown as a function of laboratory-system energy for laboratory-system angles shown. The absolute yields are indicated for the uppermost curve. Successive curves are displaced, each by one order of magnitude.

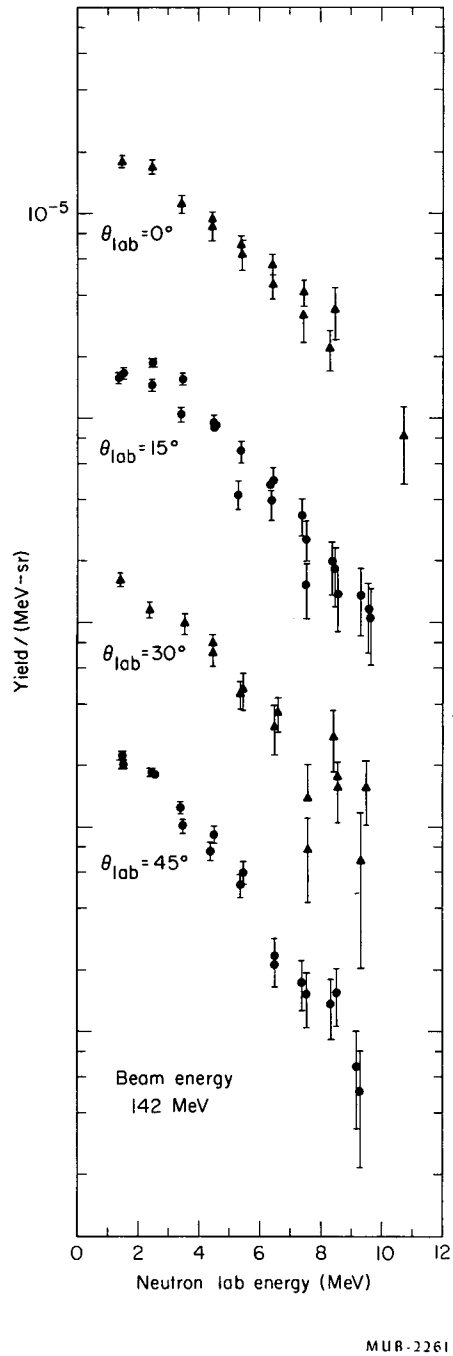

Fig. 10. Experimental results: The neutron yields are shown as a function of laboratory-system energy for laboratory-system angles shown. The absolute yields are indicated for the uppermost curve. Successive curves are displaced, each by one order of magnitude.

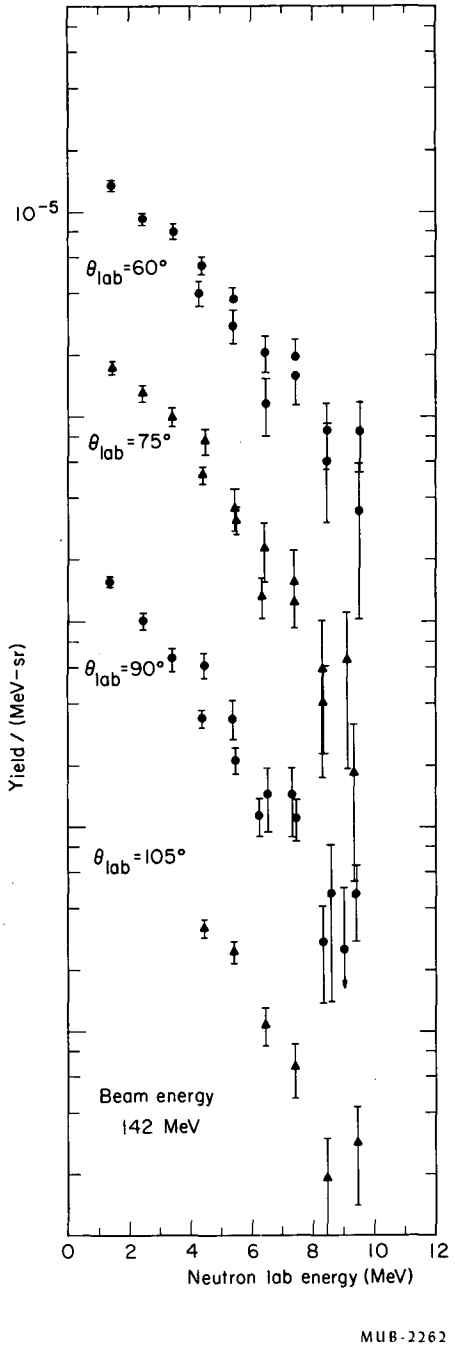

Fig. 11. Experimental results: The neutron yields are shown as a function of laboratory-system energy for laboratory-system angles shown. The absolute yields are indicated for the uppermost curve. Successive curves are displaced, each by one order of magnitude.

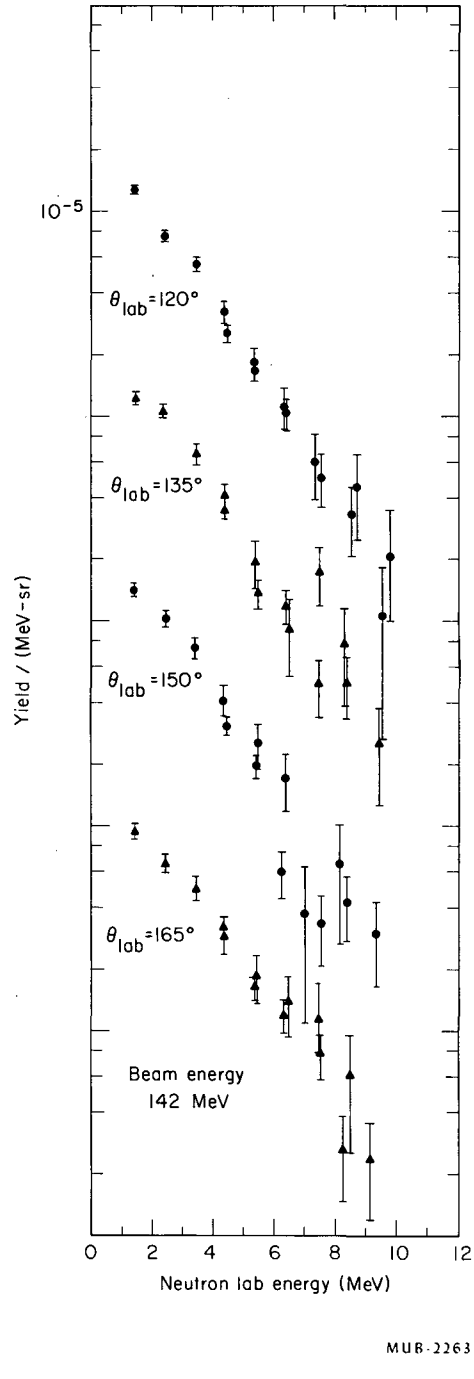

Fig. 12. Experimental results: The neutron yields are shown as a function of laboratory-system energy for laboratory-system angles shown. The absolute yields are indicated for the uppermost curve. Successive curves are displaced, each by one order of magnitude.

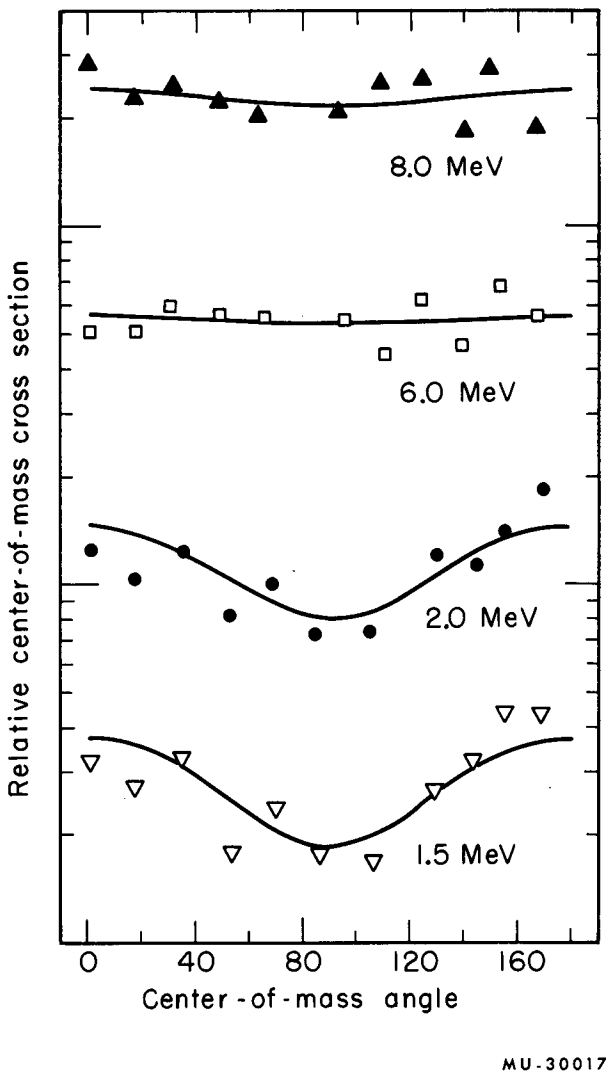

Fig. 13. Center-of-mass angular distribution for neutrons.

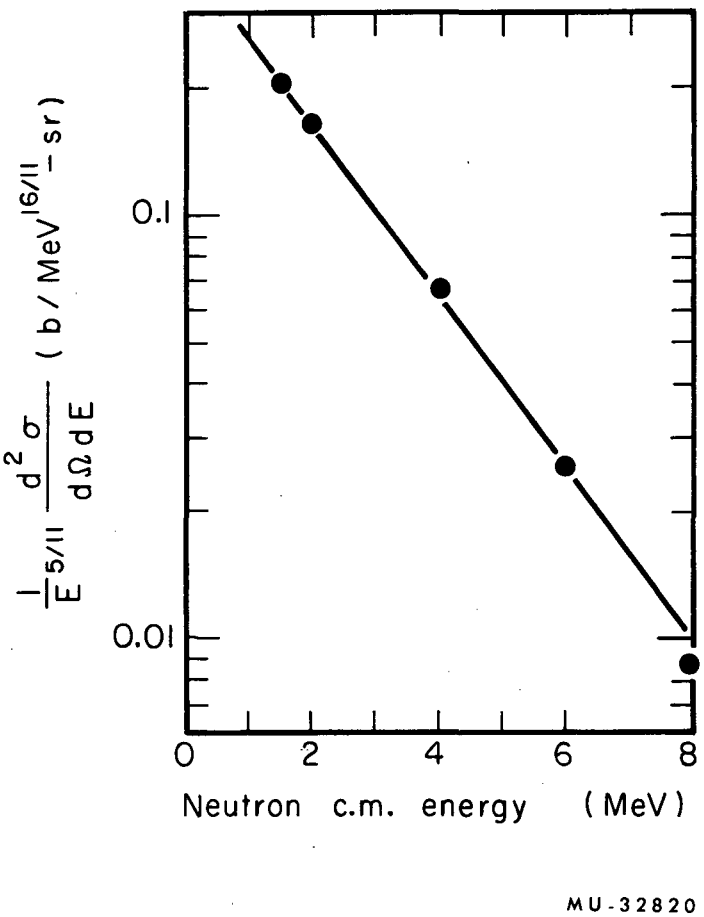

Fig. 14. "Temperature plot" assuming a center-of-mass distribution of the form given by LeCouteur [Eq. (8) of this paper]. The line shown gives

$$\frac{d^2\sigma}{d\Omega dE} = 415\, E^{5/11}\, e^{-E/2.08} \text{ mb/MeV-sr.}$$

B. Angular Distributions

There is no evidence of forward peaking. In fact, there seems to be a tendency to peak backwards. This could be a result of incomplete momentum transfer to the compound system. For those reactions with incomplete momentum transfer, the velocity of the compound system would be overestimated, with the result that neutrons would appear to be peaked backwards in the compound system. Sikkeland et al.[17] have observed that incomplete momentum transfer occurs in a significant fraction of heavy-ion-induced fission reactions.

With the nuclear evaporation theory one is able to predict the effects of angular momentum on the decay of the compound system. The density of states for the nucleus then depends on angular momentum, J, as well as on energy, and is predicted to be of the form[2]

$$\rho(U, J) = \rho(U, 0)\,(2J+1)\exp[-J(J+1)/2\sigma^2] \ ,$$

where $\sigma^2 = \mathcal{J}T/\hbar^2$; $\mathcal{J}$ and T are the moment of inertia and temperature of the residual nucleus. The parameter that describes the magnitude of the effect of angular momentum on the angular distribution is $J\ell/\sigma^2$, where ℓ is the orbital angular momentum of the emitted particle, and J is the spin of the initial nucleus. For $J\ell/\sigma^2 >> 1$, the angular distribution has the form

$$W(\theta^*) \propto \frac{1}{\sin\theta^*} \ .$$

For $J\ell/\sigma^2 << 1$, there results $W(\theta^*) \propto 1 + a\cos^2\theta^*$, with $a = \mu R^2 E_{rot}/2\mathcal{J}T$, where μ is the reduced mass of the particles, R is the radius of the compound nucleus, and E_{rot} is the rotational energy of the system. The distributions are more complicated for intermediate values. In our case, σ^2 is approx 340 for the first evaporation, so that the limit of small $J\ell/\sigma^2$ should be applicable. This leads to smaller values of a than those observed. The effect does, however, increase somewhat for successive evaporations because the temperature decreases. Small values of $J\ell/\sigma^2$ indicate also that there is little coupling between I and ℓ, so that only a small amount of angular momentum is removed by neutron evaporation. (Unless J and ℓ couple their directions so that

they tend strongly to be antiparallel, no angular momentum is removed from the system.) At the last evaporation stage, therefore, the angular momentum is still large. A large amount of angular momentum must be disposed of, because at the lowest energies only low-spin states are energetically available to the residual nucleus. Therefore, there are expected to be large anisotropies for the low-energy neutrons. This effect has been observed by Allen[18] and by Douglas and McDonald.[19] It could be enhanced if the last prefission neutron and the last post-fission neutron from each fragment were all strongly coupled. In this experiment, the observed anisotropy increases strongly at low neutron energies.

C. Energy Dependence of the Neutron Spectra

The spectra result from multiple emission of neutrons; that is, there are several neutrons emitted per event. Le Couteur has given approximate forms for the energy distribution of neutrons from an evaporation chain.[20] He finds for an assumed dependence of the temperature on the excitation energy, $T \propto (U)^{1/2}$, that the distribution of neutron energies has the form

$$\frac{d^2\sigma}{d\Omega dE} = \text{const} \times E^{5/11} \exp(-E/T_{eff}) , \qquad (8)$$

where T_{eff} is 11/12 of the temperature, T_{max}, governing the first evaporation. Thus, a plot of $\log (d^2\sigma/d\Omega dE)/E^{-5/11}$ vs E (Fig. 14) has slope equal to $-11/12\ T_{max}$. This gives $T_{max} = 2.27$ MeV, and for the level-density parameter a--defined in the relation $T = (aU/A)^{1/2}$--one obtains the value 9.73 MeV, which is in good agreement with the usually assumed value ($a \approx 10$ MeV). In the above, we use cross sections averaged over angle, as discussed in Section III. A. Those neutrons emitted after fission are raised in energy by an amount equal to the energy per neutron mass of the fragments. This effect has been neglected in this discussion. Also the effect of angular momentum on the energy spectra is ignored. This effect has been calculated to be small.[9]

The total cross section can be estimated by integrating the form (Eq. 8) over energy. A least-squares fit to the data points leads to the energy dependence

$$\frac{d^2\sigma_{av}}{d\Omega dE} = 415\, E^{5/11} e^{-E/2.08} \text{ mb/(MeV sr)}.$$

Upon integration, this gives a total cross section of 12.3 b. This value is quite sensitive to the assumed form of the spectrum, so that this result may well be in error by about 25% instead of the 17.5% normalization error calculated in Section II. D. This sensitivity reflects the fact that a large fraction of the neutrons are emitted with energies below the lowest energy measured in this experiment (1 MeV). The ratio of the total number of neutrons expected for these measurements to the number expected at beam energies of 164 MeV is calculated to be 0.82. In this calculation we used the cross section of Thomas[21] and assumed that one additional neutron results from an increase of 11 MeV in excitation energy. The value for comparison with experiments at 164 MeV, 15 b, lies between the values of 12.8 and 19.2 b given by Hubbard et al.[8] for carbon and neon, respectively, on Au. It is somewhat below the value of 25 ± 10 b given by Broek.[9]

D. Fission-Neutron Competition

1. Experiment

Measured angular distributions of fission fragments show large anisotropies. For 164-MeV O^{16} ions on Au, the forward-to-90-deg ratio is about four.[3,5] This anisotropy affects the angular distribution of neutrons evaporated from the fragments, and thus presents a possibility for separating pre- and postfission neutrons. The following analysis of the neutron angular distributions measured in this experiment leads to the conclusion that some neutrons are evaporated before fission occurs.

We now calculate the center-of-mass angular distribution expected for neutrons evaporated from the moving fission fragments. We assume that the neutron distribution in the fragment rest frame can be written

in the form

$$\frac{d^2\sigma}{d\Omega dE_f} = E_F^{\gamma} \exp(-E_F/T)\,(1 + a_f \cos^2\theta_F)\,, \qquad (9)$$

where θ_F is the angle between the direction of emission of the neutron and the fragment velocity, and where γ, T, and a_f are adjustable parameters. This distribution is first transformed to a coordinate system at rest in the compound system with polar axis along the direction of fragment motion. Then a rotation is made to align the polar axis with the beam direction, so that an integration over the fission-fragment distribution can be made. The details are given in Appendix III. Angular distributions were tabulated for several values of γ, T, and a_f. The calculated anisotropy increases with increasing neutron energy, and, at high neutron energies, is greater than that observed. The effect of increasing a_f was found, as expected, to increase the anisotropy. Some typical results are shown in Fig. 15. Curve D has the flattest distribution. The observed distribution at 8 MeV is flatter than that for curve D by only 1.1 standard deviations. However, this curve with T = 2.0 MeV leads to an average neutron energy of 4.7 MeV, which is considerably higher than the observed value of 3.01 MeV. To obtain agreement with the average neutron energy, one must assume a temperature of 1.5 MeV, which results in the more anisotropic curve A. This curve has a value of a that disagrees with the observed value by three standard deviations. This argument is summarized in Table III. It is seen that no value of the temperature can make both the anisotropy and the average neutron energy coincide with experiment, and thus the data are inconsistent with the assumption that all neutrons are emitted after fission occurs.

It should be stressed that this is a purely geometric transformation and that the results do not depend upon any details of evaporation theory, etc. Particularly, the "temperature" T is only a parameter that describes how fast the spectrum drops off with increasing neutron energy. It is not supposed to agree with the temperatures discussed in Section II. C.

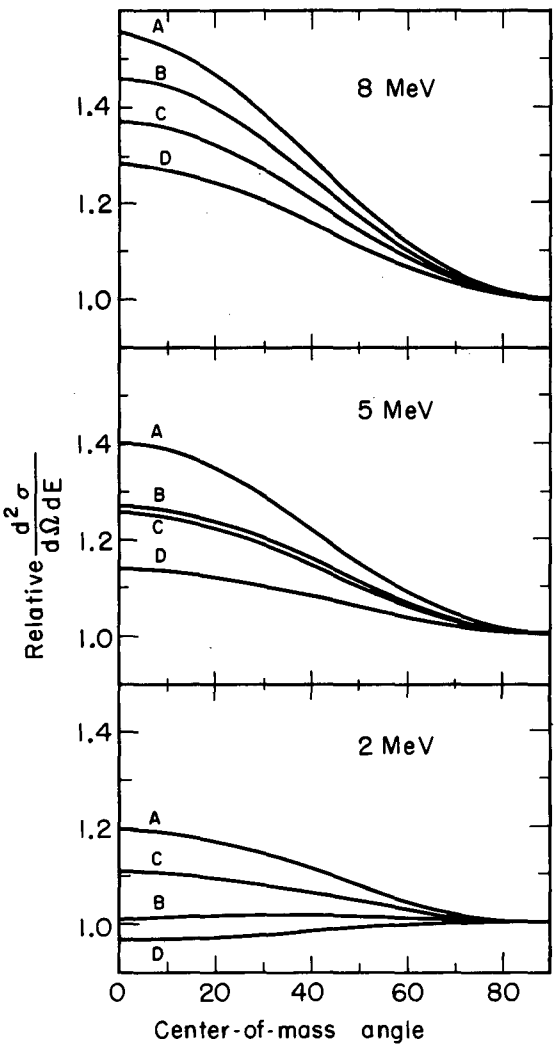

Fig. 15. Neutron angular distributions calculated assuming postfission emission. Curves A and C are for Maxwell distributions, with T = 1.5 and 2 MeV; B and D are for Weisskopf distributions at 1.5 and 2 MeV.

Table III. Comparison of calculated and observed values of the average neutron energy $\langle E_{cs} \rangle$ and anisotropy a. E is the neutron energy, T the nuclear temperature, and τ the fragment kinetic energy per neutron mass. No assumed value of T can make both $\langle E_{cs} \rangle$ and a agree with the observed values.

Assumed distribution in fragment rest frame	Mean energy in fragment rest frame	Resulting distribution in compound-system frame	Mean energy in compound-system frame $\langle E_{cs} \rangle$
Weisskopf: $F(E) \propto E e^{-E/T}$	2T	Feather	$\tau + 2T$
Maxwell: $F(E) \propto E^{1/2} e^{-E/T}$	3/2 T	Watt	$\tau + 3/2T$

$\tau = 0.71$, $F(\theta) = 1 + a \cos^2\theta$

	$\langle E_{cs} \rangle$	a (8 MeV)
Curve A, Maxwell, 1.5 MeV	2.96	0.56
Curve B, Weisskopf, 1.5 MeV	3.71	0.46
Curve C, Maxwell, 2.0 MeV	3.71	0.37
Curve D, Weisskopf, 2.0 MeV	4.71	0.28
Observed value	3.01	0.099±0.158

It has been argued that the angular distribution of the high-energy neutrons should not be affected by the small velocities of the fragments from which they came, and should be nearly isotropic. This is not necessarely the case. The anisotropy results because a given laboratory energy E corresponds to a higher value of E^* at 90° than at 0°. As is shown below, the quantity that characterizes the magnitude of the anisotropy is $2(E\tau_f)^{1/2}/T$, where E is the laboratory energy at which neutrons are being observed, and τ_f is the energy of the fragment divided by its mass in units of the neutron mass. Only if this quantity is small compared with unity is the distribution isotropic. For fixed values of the temperature and the fragment velocity, the anisotropy increases with the neutron energy. The following calculations shows this explicitly. Consider a nucleus with kinetic energy per neutron mass τ_f,

and assume for simplicity that neutrons are being evaporated isotropically with the energy dependence

$$\frac{d^2\sigma}{d\Omega dE^*} \propto (E^*)^{1/2}\, e^{-E^*/T};$$

then, using the transformation factor (Eq. 6), we have

$$\frac{d^2\sigma_{lab}}{d\Omega dE} = \left(\frac{E}{E^*}\right)^{1/2} E^{*1/2}\, e^{-E^*/T}$$

$$= E^{1/2} \exp\left\{\frac{-[E+\tau_s - 2(E\tau_s)^{1/2}\cos\theta]}{T}\right\},$$

and we have for the ratio of the cross section at 0 deg to the 90 deg cross section

$$\frac{d^2\sigma_{lab}}{d\Omega dE}\Big|_{0°} \Big/ \frac{d^2\sigma_{lab}}{d\Omega dE}\Big|_{90°} = \exp\{[2(E\tau_s)^{1/2}]/T\}.$$

Thus the higher the laboratory-system neutron energy, the more forward-peaked is the neutron angular distribution. This result does not depend on the detailed shape of the assumed center-of-mass distribution. It shows why the conclusion--that some neutrons are not coming from moving fragments--is supported most clearly by examining the angular distributions of these neutrons at high energies.

2. Theory

The problem of neutron-fission competition has recently been extensively discussed by Huizenga and Vandenbosch,[22] who give for the ratio Γ_n/Γ_f the expression

$$\Gamma_n/\Gamma_f = \frac{4A^{2/3}(U-B_n' - E_R)}{K_0[2a^{1/2}(U-E_f'-E_R^f)^{1/2}-1]} \times \exp\left\{2a^{1/2}[(U-B_n'-E_R)^{1/2} - (U-E_f'-E_R^f)^{1/2}]\right\}, \quad (10)$$

where U is the excitation energy of the compound system,

A is the atomic mass,

B_n' is the neutron-binding energy corrected for pairing and shell effects,

E_R is the rotational energy of the equilibrium nucleus,

E_R^f is the rotational energy of the saddle-point configuration,

E_f' is the fission barrier for a nonrotating nucleus corrected for odd-even effects,

a is the level-density parameter,

$K_0 = \hbar^2/2mr_0^2$,

and m is the neutron mass.

In this equation one assumes a level density of the form $\rho=\exp[2(aU)^{1/2}]$, with the same value of a for the level density of the saddle-shaped nucleus as for the neutron-emitting nucleus. R. Vandenbosch et al.[23] found it necessary to assume different values of a for the saddle-shaped and neutron-emitting nucleus in the interpretation of their results from the bombardment of heavy elements with 23 to 40-MeV α particles. However, they conjecture that at higher excitations (such as those involved in this experiment) this difference should disappear. In the following analysis, we use the commonly assumed value $a = A/10$ per MeV. The quantities $A^{2/3}$ and $a^{1/2}$ do not change much during the course of an evaporation chain. It is convenient to consider them as constants. The ratio Γ_n/Γ_f then depends on just two variables: The first may be taken to be the excitation energy in excess of the saddle-point energy, $Q \equiv U - (E_f' + E_R^f)$, and the second may be taken to be a quantity characteristic of the competition process, $E_n^f \equiv (B_n' + E_R) - (E_f' + E_R^f)$. This is analogous to the quantity $B_n' - E_f'$ considered in fission-neutron competition without angular-momentum effects.[22]

The nucleus at the high excitation considered here should be essentially free from shell and pairing effects, and therefore the shell and pairing corrections given by Cameron[24] were subtracted from the masses given in the appendix of that work; that is, the masses used agree with Eq. (7) of reference 24. The resulting neutron-binding energies are a smooth function of A and Z, and in the region of interest were found to fit well the empirical form

$$B_n'(Z,A) = 8.36 - 0.0888\,[12.06 - 2.906Z + 2(A-Z)],$$

which was used in these calculations.

The quantity $E_f' + E_R^f$ represents the energy of the saddle-point nucleus that is unavailable for intrinsic excitation. In using this expression (Eq. 10), one assumes that the surface and Coulomb energies of the saddle shape are not affected by angular momentum. This approximation is good only for small angular momenta. For large angular momenta, a more realistic expression for the unavailable energy is $E_{fR} + E_R$, where E_{fR} is the fission threshold energy of the rotating nucleus. For numerical values of E_{fR} and E_R, we use the results of liquid-drop calculations recently made by Cohen, Plasil, and Swiatecki.[25] Making these substitutions, we have

$$E_n^f = B_n' - E_{fR},$$

and the expression [Eq. (10)] for Γ_n/Γ_f becomes

$$\Gamma_n/\Gamma_f = \frac{\text{const}\times(Q-E_n^f)}{2a^{1/2}Q^{1/2} - 1} \exp\left\{2a^{1/2}\left[(Q-E_n^f)^{1/2} - Q^{1/2}\right]\right\},$$

where a is now assumed to be constant, so that E_n^f and Q are the only two independent variables.

In the approximation considered here, a nucleus is completely specified by its charge Z, its mass A, its angular momentum J, and its excitation energy U, so that E_n^f depends only on Z, A, and J. Figures 16 and 17 show the dependence of E_n^f on A and J for $Z = 87$ and $Z = 85$. Figures 18 and 19 then show the dependence of Γ_n/Γ_f on E_n^f and Q. A compound nucleus is formed with $Q \approx 100$ MeV and, with each neutron evaporation, moves to the left a distance $B_n' + E_{kinetic} + \delta$ on the figure; δ is a small quantity that represents changes in rotational energy and in the fission barrier resulting from the emission of a neutron. The probability that it fissions after each neutron emission is given by its position on Fig. 18. Its ordinate, E_n^f, at any time is given by reference to Fig. 16. Typical average paths are shown in

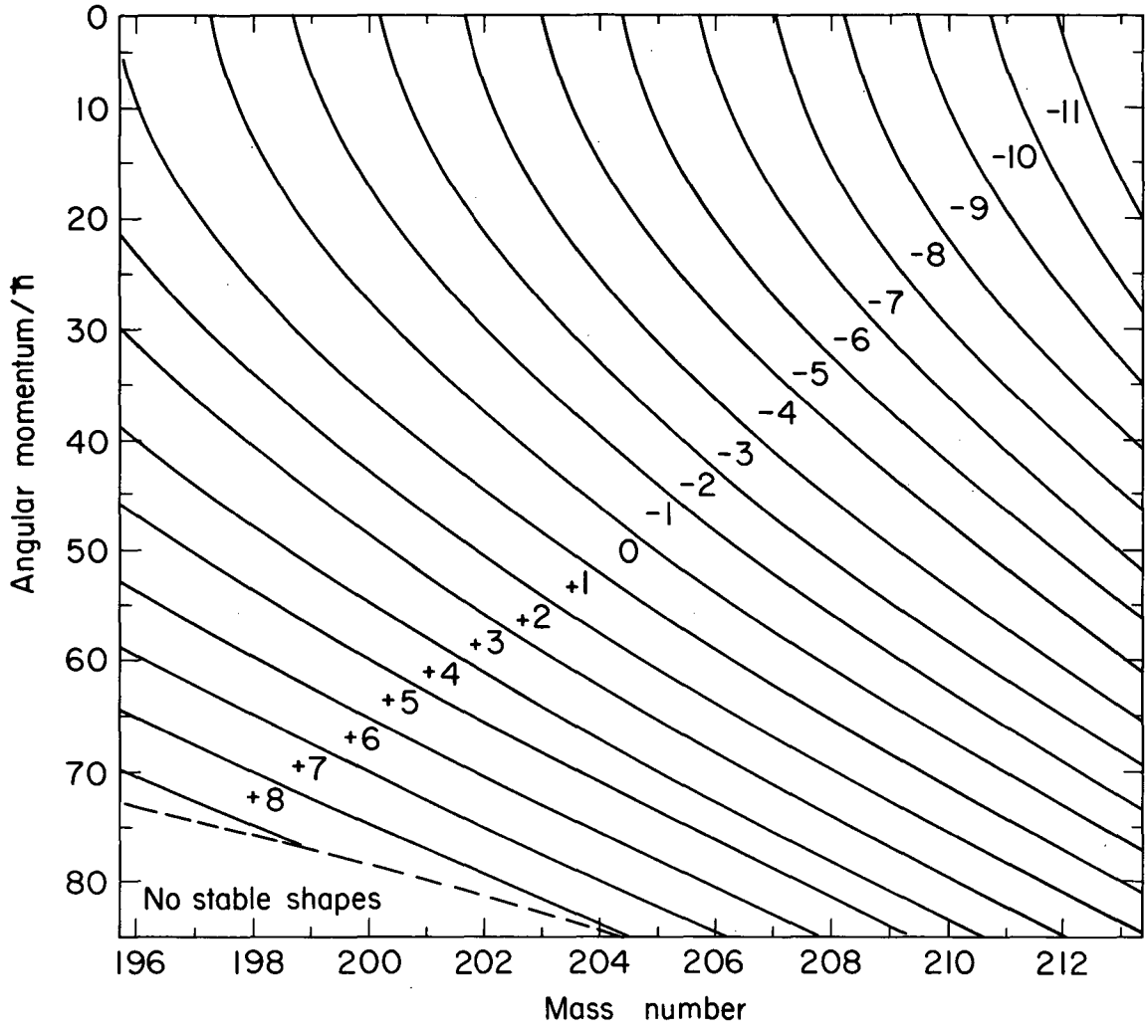

Fig. 16. Values of the difference between the neutron binding energy and the fission barrier, E_n^f, as a function of the mass number A and the angular momentum J of the compound nucleus. The curves are contours of equal values of E_n^f. The value of E_n^f in MeV is shown beside the contours. $Z = 87$. The strong dependence of E_n^f on A reflects the strong dependence of the fission barrier on the fissionability parameter Z^2/A, and shows why Γ_n/Γ_f decreases with each neutron emission.

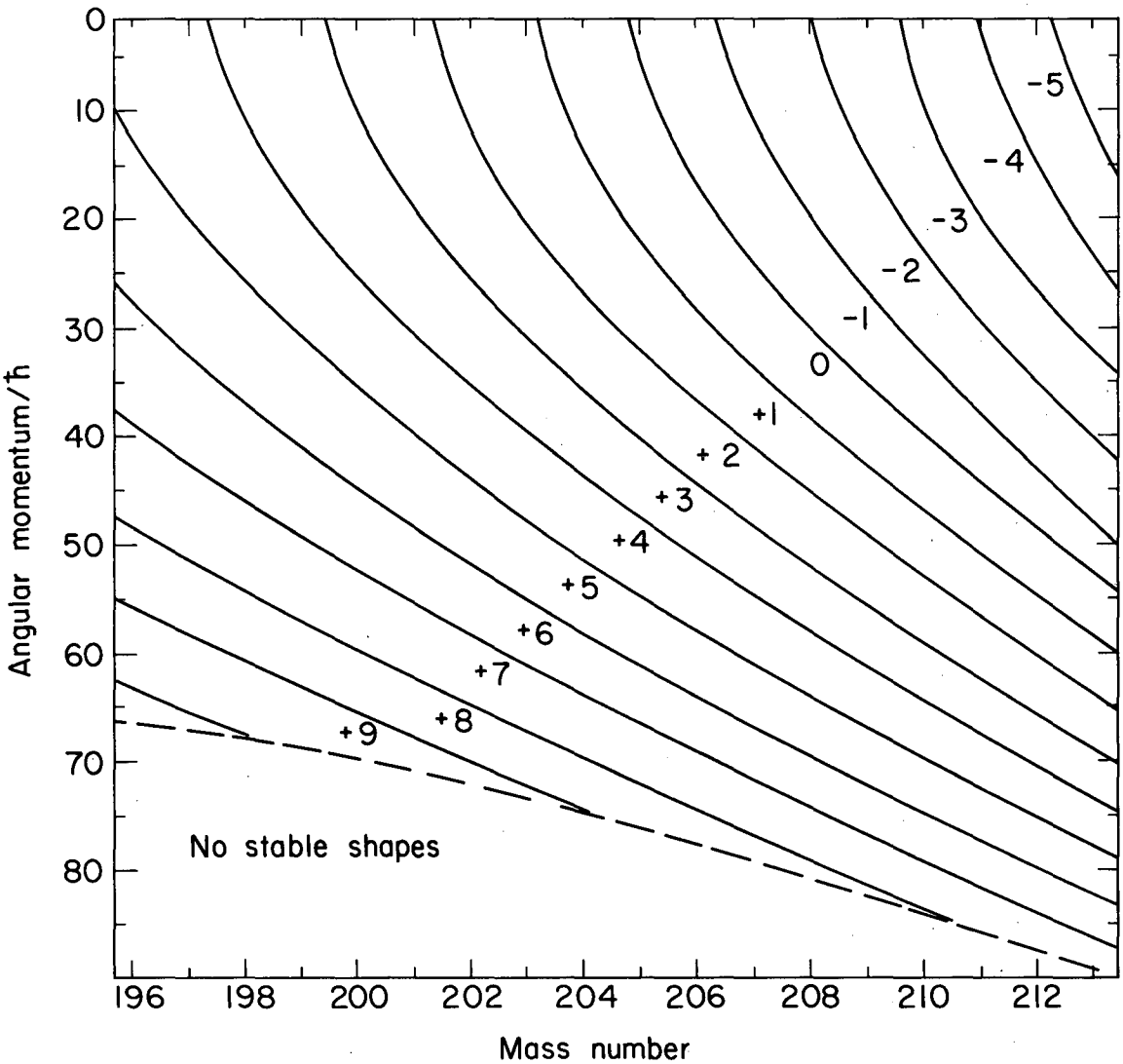

Fig. 17. Values of the difference between the neutron binding energy and the fission barrier, E_n^f, as a function of the mass number A and the angular momentum J of the compound nucleus. The curves are contours of equal values of E_n^f. The value of E_n^f in MeV is shown beside the contours. Z = 85. The strong dependence of E_n^f on A reflects the strong dependence of the fission barrier on the fissionability parameter Z^2/A, and shows why Γ_n/Γ_f decreases with each neutron emission.

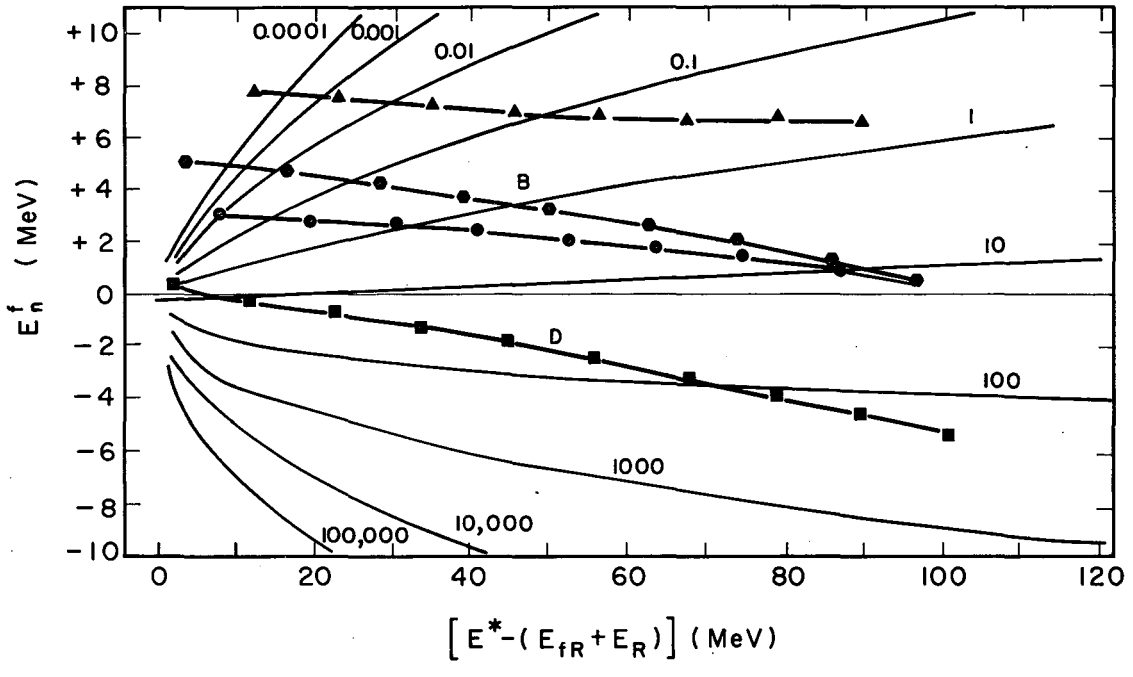

Fig. 18. The solid curves without points are contours of equal values of the parameter Γ_n/Γ_f. The lines with points indicate "trajectories" for typical nuclei under various assumptions, as follows: Z = 87; Curve A: initial L = 85, ΔL = -2; Curve B: initial L = 57, ΔL = 0; Curve C: initial L = 57, ΔL = -2; Curve D: initial L = 5, ΔL = 0.

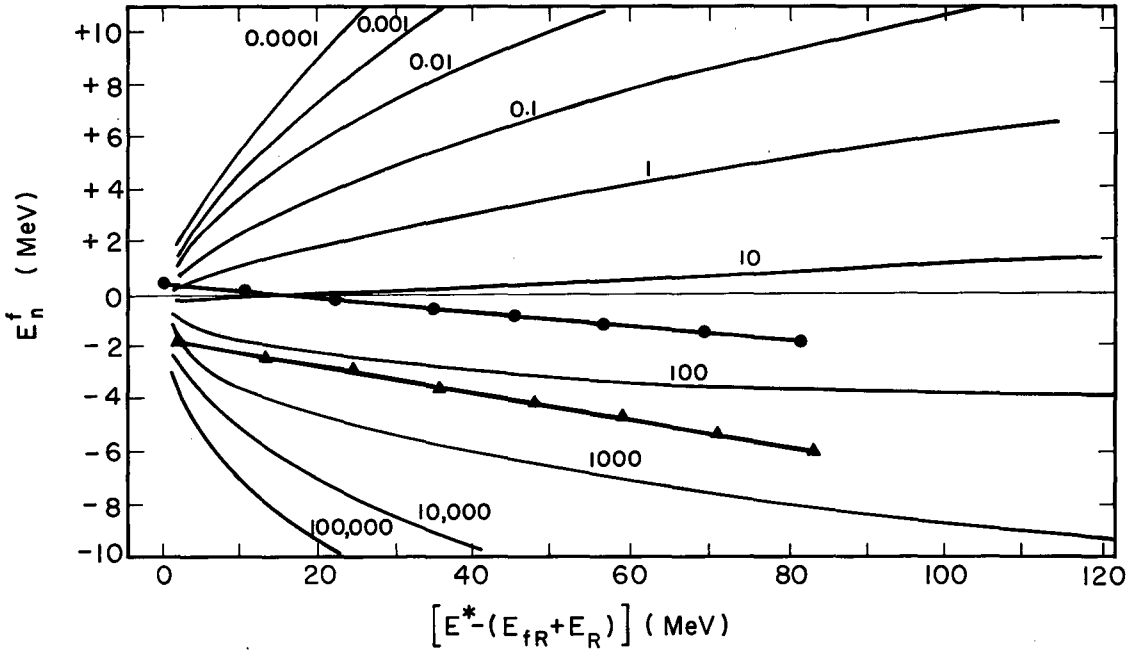

Fig. 19. The solid curves without points are contours of equal values of the parameter Γ_n/Γ_f. The lines with points indicate "trajectories" for typical nuclei under various assumptions, as follows: Z = 85; Upper curve: initial L = 55, ΔL = -2; Lower curve: initial L = 40, ΔL = -2.

Fig. 18. For the curve C, for instance, one assumes an initial J of 57 (this is the average initial value of J), and one assumes also that 2 units of angular momentum are removed with each neutron evaporation.

The average angular momentum removed in the process of emitting a neutron is not well established at the present time. A theoretical estimate can be made if a level density for rotating nuclei is assumed. For a level density of the form

$$\rho(U, J) = (2J+1)\rho(U,0) \exp(-J^2/2\sigma^2),$$

the average angular momentum removed by the first neutron is about $1/2\,\hbar$. (This value was determined from a computer program written by Donald V. Reames.) Calculations are made here for an average value of angular momentum removed of 0 and $2\hbar$ to illustrate the dependence of Γ_n/Γ_f on this quantity. It is very unlikely that the average angular momentum removed by a neutron is greater than two, because such a large value leads to the conclusion that the neutron angular distribution is highly peaked in the forward and backward directions, contrary to experiment.

The series of points on the graph (Fig. 18) at which successive neutron emissions of a single nucleus occur define a trajectory. When fission occurs, the trajectory ends. The probability of fissioning on the Nth chance is

$$P_N = \Pi_{j=1}^{N-1}(1-W_j)W_N,$$

where $W_N = \dfrac{1}{1+\Gamma_n/\Gamma_f}$, and the average number of neutrons emitted before the nucleus fissions is

$$\bar{n} = \sum_{N=1}^{n_{max}} (N-1)\, P_N. \qquad (12)$$

Since the initial distribution of angular momentum and excitation energies is approximately known, it would be possible to carry out Monte Carlo calculations to determine such quantities as the distribution of

the number of neutrons emitted and their energy distribution. However, because of the uncertainties in the theoretical parameters involved, etc., it seems sufficient to consider only a few representative evaporation chains. First, consider a nucleus with angular momentum equal to the average value for all nuclei (57$\hbar$), and assume that each neutron carries away 2 units of angular momentum. The "trajectory," under these assumptions, is the curve C in Fig. 18. The average number of neutrons emitted before fission is 4.04. Nearly all nuclei fission, and most of them fission after the emission of several neutrons. The value E_n^f increases with each neutron emission, and thus fission becomes more and more likely at successive steps in the evaporation chain. This increase in E_n^f is caused primarily by the increased fissionability of the nucleus as its mass decreases. The small increase ($\approx 1/2\%$) in the fissionability parameter, Z^2/A, with the emission of a neutron influences greatly the neutron-fission competition process, as can be seen by examining the effect of this on E_n^f (Fig. 16). This together with the consideration (see Fig. 18) that neutron emission is preferred at high excitation energies--even if E_n^f is somewhat greater than 0--explains why neutron emission is favored at the beginning of the evaporation chain even though nearly all nuclei eventually fission. The dominance of neutron emission over fission at very high energies has been discussed by Perfilov et al.[26]

Another factor that enters the overall picture for this reaction is the high cross section for direct α emission, measured to be 0.54 b by Britt and Quinton.[1] Assuming that these alphas are involved singly and do not result from, for example, the breakup of a carbon nucleus into three alphas, then about 1 in 4 reactions involve a compound nucleus with Z = 85 instead of Z = 87. For this reason the dependence of Γ_n/Γ_f was calculated for Z = 85 (see Fig. 19) as well as for Z = 87. The difference between these two cases is very great. In the Z = 85 case, only about half the nuclei fission. This agrees with the measured fission cross section of 0.9 b from the bombardment of Au by 120-MeV C^{12} ion, which is approx 45% of the total cross section.[3]

Table IV summarizes the results of these calculations by giving the probability of fission at the Nth chance for various assumptions about the initial conditions and the amount of angular momentum removed by neutron emission.

Table IV. Values of the probability that a nucleus fissions on the Nth chance under the assumptions listed at the top of each column. Z is the nuclear charge, J the initial angular momentum, and ΔJ is the average amount of angular momentum removed per neutron emission. The initial mass number A is 213 for Z = 87 and 209 for Z = 85. Across the bottom of the table are listed the mean number of neutrons, $\bar{n}$, emitted before fission occurs.

J	Z = 87	Z = 87	Z = 87	Z = 87	Z = 85	Z = 85
	J = 57	J = 57	J = 5	J = 85	J = 55	J = 40
	$\Delta J = 0$	$\Delta J = -2$	$\Delta J = 0$	$\Delta J = -2$	$\Delta J = -2$	$\Delta J = -2$
N	Curve B Fig. 17	Curve C Fig. 17	Curve D Fig. 17	Curve A Fig. 17	Upper curve Fig. 18	Lower curve Fig. 18
1	0.071	0.071	0.005	0.645	0.024	0.0031
2	0.106	0.0845	0.007	0.262	0.030	0.0037
3	0.142	0.111	0.009	0.0745	0.034	0.0043
4	0.184	0.122	0.012	0.017	0.036	0.0050
5	0.216	0.134	0.106	0.0023	0.046	0.0055
6	0.207	0.176	0.025		0.063	0.0059
7	0.107	0.166	0.04		0.085	0.0055
8	0.020	0.105	0.05		0.68	0.0001
9	0.001	0.028	0.06			No fission
10	----	----	0.88			No fission
$\bar{n}$	3.62	4.04	9.24	0.471	6.06	7.85

APPENDIX I.

A. External-Radiator Calculations

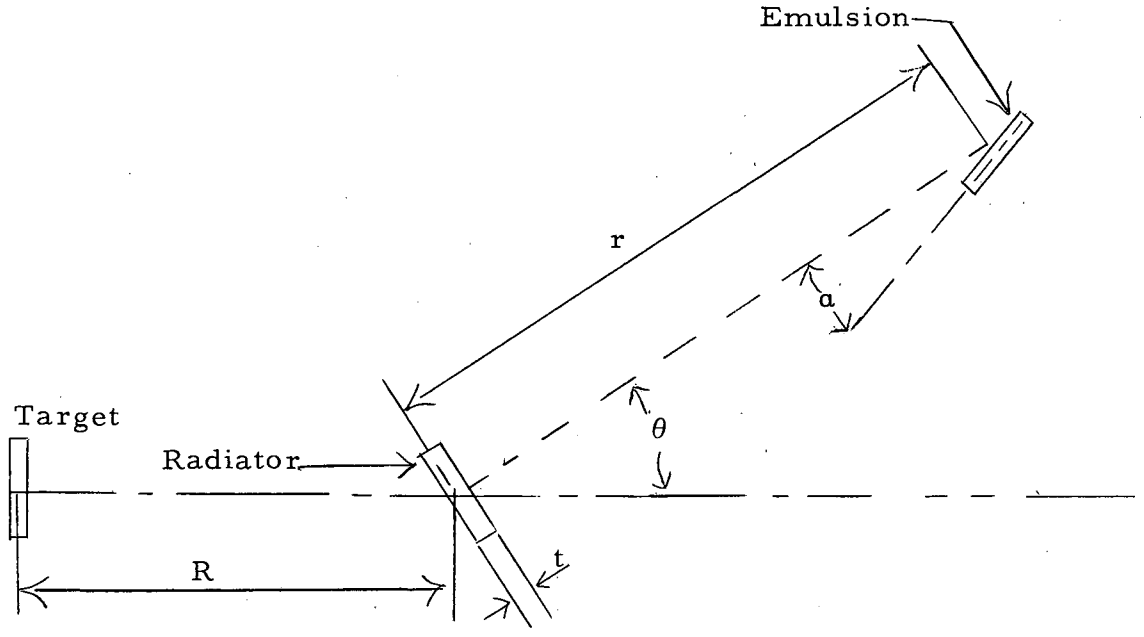

In this appendix, we derive formulas for the neutron cross section for the external-radiator method. First assume a radiator of small area and thickness. The double differential cross section for S-wave scattering of protons by neutrons can be written as

$$\frac{d^2\sigma}{d\Omega dE} = \frac{d\sigma_{np}}{dE}\,\frac{\cos\theta}{\pi} \quad ,$$

where $d\sigma_{np}/dE$ is the total np cross section, and θ is the angle between the initial direction of the neutron and the proton direction. Then we have for the number of protons $d^2N/d\Omega dE$ observed per unit solid angle with energy between E and $E+\Delta E$,

$$\frac{d^2N}{d\Omega dE}dE = \frac{dN_0}{dE'}\,N_r\,\frac{\cos\theta}{\pi}\,\frac{d\sigma_{np}}{dE'}\,dE' \quad .$$

Here, E' is the energy of the neutron, which, upon colliding, produces a proton of energy E at the detector, and dN_0/dE' is the number of neutrons per cm^2 with energies between E' and $E'+dE'$ at the radiator,

and N_r is the total number of protons in the radiator. If the surface area of the emulsion scanned for protons is A, then the solid angle of acceptances is $A/r^2 \sin\alpha$, where r^2 and α are as shown. The flux at the radiator is then

$$\frac{dN_0}{dE'} = \frac{\frac{dN}{dE}\,\frac{dE}{dE'}\,r^2 \sin\alpha}{N_r \frac{d\sigma_{np}}{dE}\,\frac{\cos\theta}{\pi}\,A} \quad . \tag{13}$$

We now examine the factor dE/dE'. For E, we can write $E=E'\cos^2\theta - E_L$, where E_L is the energy that the proton loses in passing through that part of the radiator left to be traversed and through the aluminum degrading foil. Then

$$dE = dE'\cos^2\theta - \frac{dE_L}{dE'}\,dE' \quad .$$

The energy loss dE_L is a function of E', which decreases with increasing energy, so that dE_L/dE' is negative. We write, then,

$$\frac{dE}{dE'} = \cos^2\theta + \gamma \quad ,$$

with $\gamma > 0$. Numerical values for γ were found by computing the energy loss for protons traveling through the polyethylene radiator and through the aluminum shield, and observing the change ΔE in E for changes $\Delta E'_p$ in E'_p; E'_p is the initial energy of the proton. For these purposes, it is adequate to assume that all protons originate at the center of the radiator.

APPENDIX II.

A. Multiple Scattering of Protons With Energy Loss

In this appendix, measurements of the shape of proton tracks in nuclear emulsion are reported, and compared with calculations by Barkas.[27] The value of the "scattering factor", K_0, for low-velocity protons ($\beta < 0.3$) is obtained empirically, and compared with values obtained from Molière's theory. Finally, the results of these measurements are used to obtain corrections for protons leaving an emulsion plate, which are necessary in the internal recoil method of neutron detection.

1. Measurements

Measurements were made on a beam of stopping protons entering a 600-μ Ilford G 5 pellicle parallel to its surface. The coordinates of the track were recorded at intervals along the track, determined as follows: The interval is taken to be 100 μ unless a visible change in direction (≈ 2 deg) occurs, in which case the interval is divided until this criterion is met. No attempt was made to determine the details of the track ending (the last approx 200 μ of track). From these sets of points, the following quantities describing the shape of stopping tracks were calculated as a function of the parameter R_p, which is the projection of the track range on its initial direction:

a. $\langle y \rangle$ and $\langle y^2 \rangle$, where y is the lateral displacement of the track;

b. $\langle R - R_d \rangle$ and $\langle (R - R_d)^2 \rangle$, where R is the "true range," defined here as the sum of the measured range segments, and R_d is the direct or "crow" range;

and c. $\langle R_d - R_p \rangle$ and $\langle (R_d - R_p)^2 \rangle$.

Tracks with large single scatterings (> 4 deg) were not included in this analysis. The effects of this are discussed in a later section. The initial direction of the track is defined by the first two points of the track. The error in the initial direction of the track is thus approx 1 deg. Although this significantly affects the value of y for a single

track, the averages $\langle y \rangle$ and $\langle y^2 \rangle$ should not be strongly affected because this error is random. In the worst cases, this amounts to an overestimation of $\langle y^2 \rangle$ by about 5%. A single proton track is used to obtain values of y, and the other track parameters for several values of R_p. The points of the track beginning with the track ending, are recorded. When R_p exceeds one of the values $n \times 0.5$ mm, that point of the track is considered to be the origin, and the track parameters are calculated.

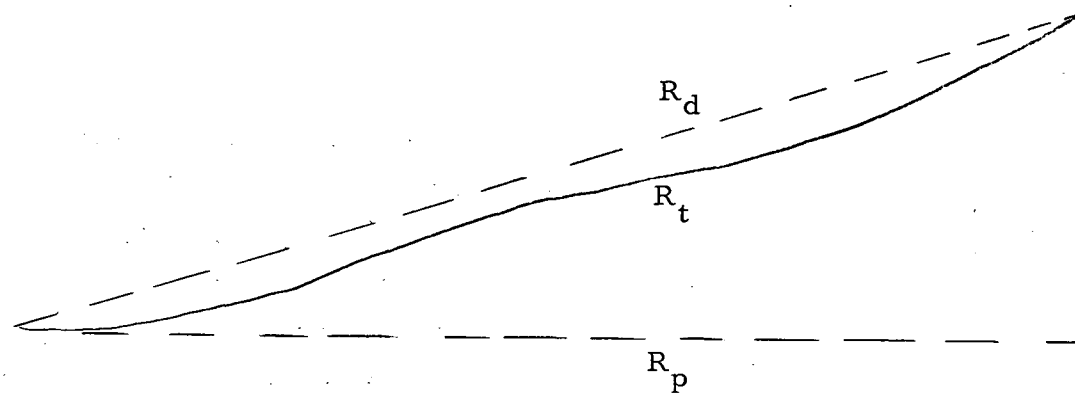

2. Results and Discussion

The increase in the mean-square projected scattering angle $\langle \phi^2 \rangle$ is closely represented by the expression

$$\frac{d\langle \phi^2 \rangle}{dt} = \frac{K_0^2 Z^2}{2p\beta c} , \tag{14}$$

where Z is the charge of the particle, $p = M\beta\gamma c$ is its momentum, and βc is its velocity. The constant K_0^2 is determined in a later part of this Appendix with the use of Molière's theory of multiple scattering.

Barkas[27] used Eq. (14) and a range relation that takes the form

$$P\beta c = 0.44 Z^{6/5} M^{2/5} R_p^{3/5}, \tag{15}$$

where M is in units of the proton mass and R_p is in microns, to obtain explicit relations for the track parameters measured in this work. He derives the following results:

$$\langle y^2 \rangle = \frac{a}{18} Z^{-2/5} M^{-4/5} R_p^{9/5}, \tag{16}$$

$$\langle R - R_p \rangle = \frac{a}{16} \left(\frac{R_p}{Z^{1/2} M} \right)^{4/5} \tag{17}$$

and

$$\langle R - R_d \rangle = \frac{5}{72} a \left(\frac{R_p}{Z^{1/2} M} \right)^{4/5}, \tag{18}$$

where $a = 5 \left(\frac{K_0}{0.44} \right)^2$.

According to Eq. (16), the quantity $\langle y^2 \rangle / R_p^{9/5}$ should be independent of R_p. In Fig. 20 the experimental values of $\langle y^2 \rangle / R_p^{9/5}$ are plotted against R_p. The data are consistent with Eq. (16) and give $K_0 = 0.105 \pm 0.005$ $(\text{MeV}/\mu)^{1/2}$, or $a = 0.282$ (MeV/μ). In Figs. 21 to 23 are shown the measured values of $\langle y^2 \rangle$, $\langle R - R_p \rangle$, and $\langle R - R_d \rangle$ together with curves, calculated with $K_0 = 0.105$. In all cases the agreement is satisfactory.

3. Calculation of K_0 from Molière's Multiple-Scattering Formula

We begin by describing Molière's theory, which is fully discussed in references 28 and 29. We introduce an angular unit χ_c, called the characteristic angle. For a pure element, we have

$$\chi_c^2 = \frac{4\pi N t e^4 Z(Z+1) z^2}{(p\beta c)^2}, \tag{19}$$

where N is the number of atoms per unit volume, t is the thickness of the scatterer; Z and z are the charge numbers of the stopping material and the particle, respectively.

For a composite material, such as nuclear emulsion, a sum is taken over the constituent elements. Next we wish to define an expansion parameter B through the two relations.

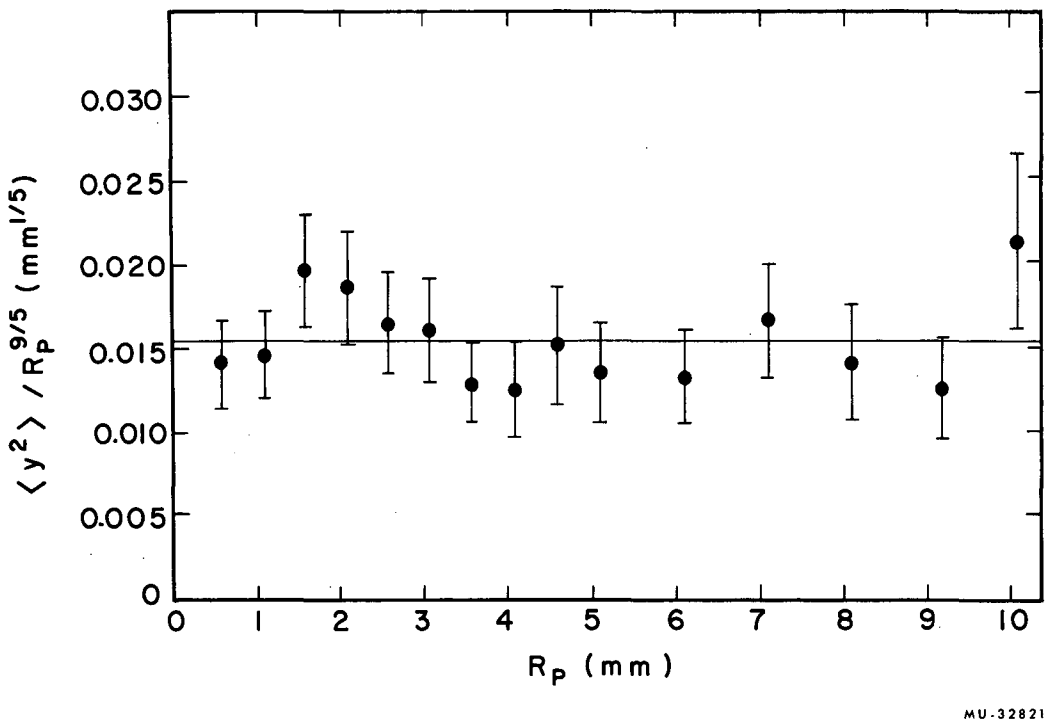

Fig. 20. $\langle y^2 \rangle / R_p$ vs R_p; the ordinate should not depend on R_p. The line shown is the average value of $\langle y^2 \rangle / R_p$.

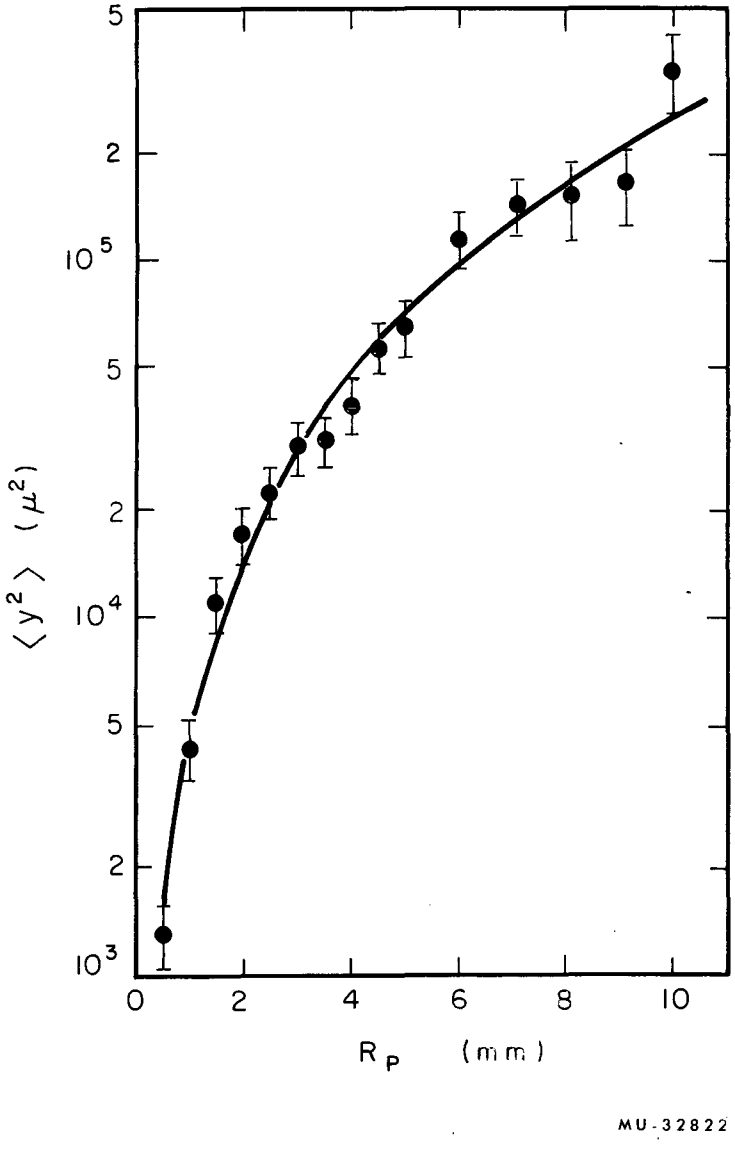

Fig. 21. $\langle y^2 \rangle$ vs R_p; the curve shown is of the form $\langle y^2 \rangle = \frac{5}{18} a R_p^{9/5}$ with $a = 0.282$.

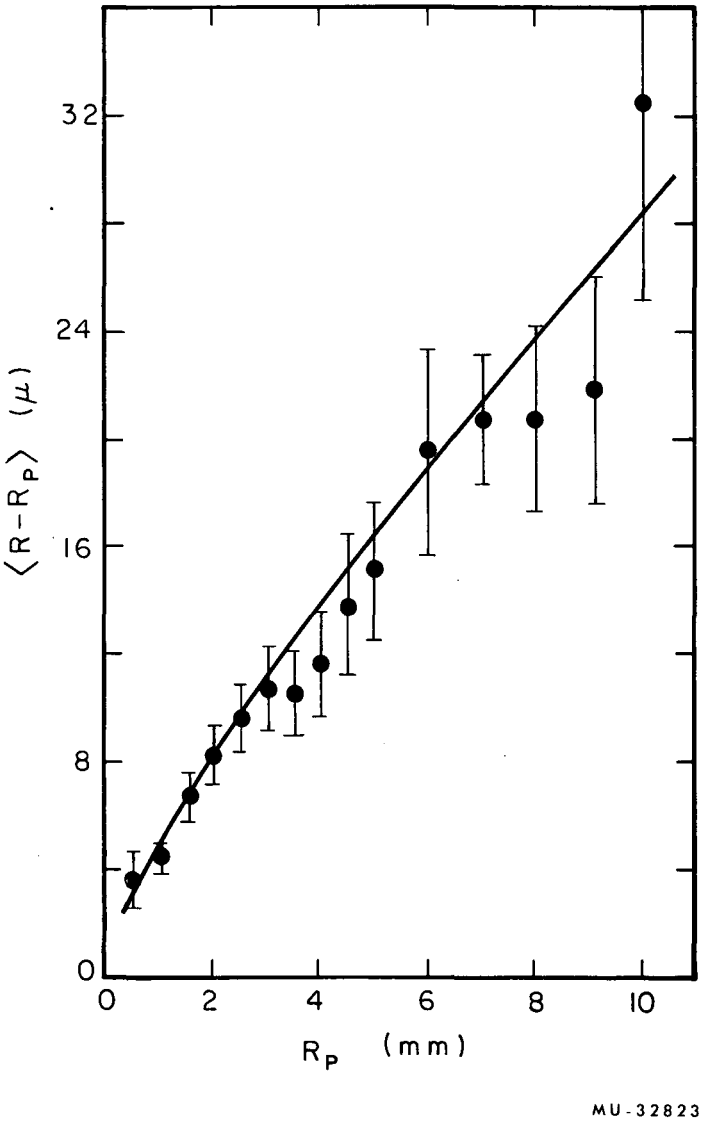

Fig. 22. $\langle R - R_p \rangle$ vs R_p; the curve shown is $\langle R - R_p \rangle = \frac{5}{16} a R_p^{4/5}$ with $a = 0.282$.

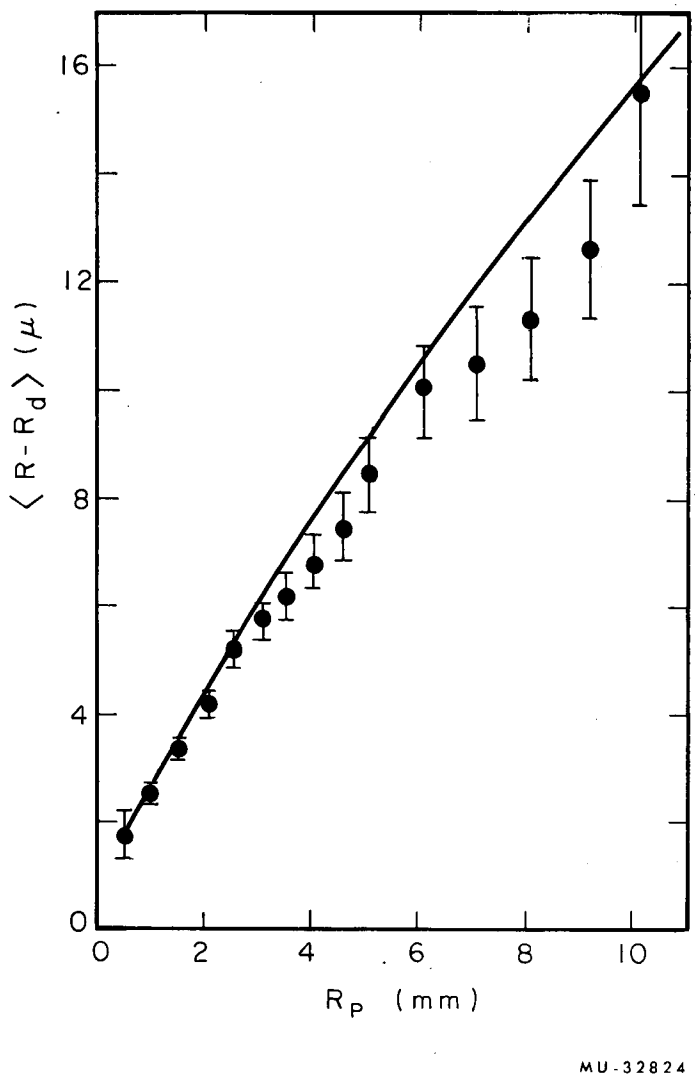

Fig. 23. $\langle R - R_d \rangle$ vs R_p; the curve shown is $\langle R - R_d \rangle = \frac{.25}{144} \alpha R_p^{4/5}$.

$$e^b = \frac{6680t(Z+1)Zz^2}{\beta^2 A\left[1+3.34\left(\frac{zZe}{\hbar c}\right)\right]^2} \quad \text{and} \quad Be^B = e^b.$$

Again, e^b is taken to be a sum over the constituent elements of nuclear emulsion. Then the scattering distribution for the reduced angle $\phi_r = \phi/\chi_c(B)^{1/2}$ is given by Molière in the form

$$f(\phi_r)d\phi_r = d\phi_r\left\{\frac{2}{(\pi)^{1/2}}\exp(-\phi_r^2) + \frac{1}{B}f^{(1)}(\phi_r) + \frac{1}{B^2}f^{(2)}(\phi_r) + \ldots\right\} . \quad (20)$$

This expression is valid for $B > 4.5$. The functions $f^{(1)}$ and $f^{(2)}$ are tabulated by Molière. The quantity B increases with the thickness t, so that for thick foils one predicts a Gaussian distribution. The rate of increase in the mean-square scattering angle, calculated over a distance Δt along the track direction with a cutoff angle ϕ_{max}, is

$$\frac{d\langle\phi^2\rangle}{dt} = \frac{\chi_c^2 B \int_0^{[\phi_{max}/\chi_0(B)^{1/2}]} f(\phi_r, t)\phi_r^2 d\phi_r}{\Delta t} \quad (21)$$

The independence of $d\langle\phi^2\rangle/dt$ on Δt is only approximate because the cutoff angle, θ_{max}, should apply to single scatterings and not to a distribution over a finite interval, Δt. The interval, Δt, should be chosen large enough to insure the applicability of Eq. (20), and small enough so that the cutoff angle is not seriously affected. A distance of 2 μ was chosen. Calculations also were done for $\Delta t = 10\,\mu$ to observe the resulting change in $d\langle\phi^2\rangle/dE$. It was found to be generally less than 1%. Results of the calculations for $K_0[\equiv (1/2p\beta c)(d\langle\phi^2\rangle/dt)]$ are shown in Fig. 24. The curves for different values of the proton energy can be brought into approximate congruence if the cutoff angle is scaled by χ_c, i.e., if we choose for the abscissa the variable ϕ_{max}/χ_c. The dependence of K_0 (or $d\langle\phi^2\rangle/dt$) on ϕ_{max} is somewhat less than logarithmic for large values of ϕ_{max}. For $\phi_{max} = 4$ deg, the calculated average value of K_0 is 0.117, which is to be compared to the measured value of 0.105 ± 0.005.

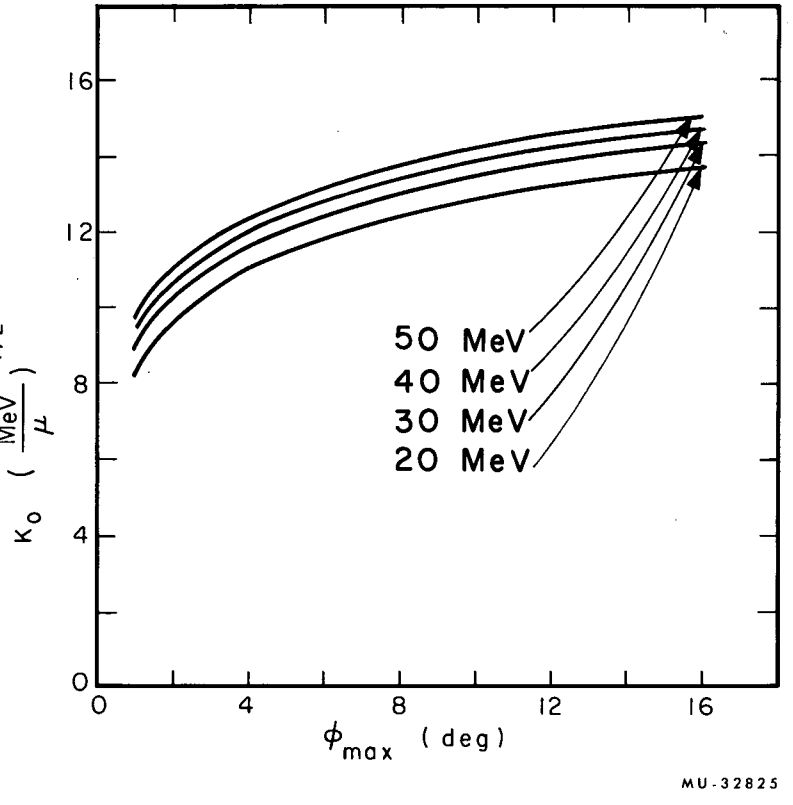

Fig. 24. Dependence of K_0, as calculated, on proton energy and on ϕ_{max}. The curves for different proton energies are brought into approximate congruence if the abscissa is changed to $\frac{\phi_{max}}{\chi_c}$, where χ_c is Moliere's "characteristic angle."

4. Evaluation of the Escape Probability for Protons in Nuclear Emulsion

a. Straight-track approximation

We consider the case of neutrons entering an emulsion plate parallel to its surface, and begin with the constraint (which is later relieved) that the recoil protons travel in straight lines until they either come to rest in the emulsion or escape from it. Define the following quantities. Here, θ equals the angle between the neutron and proton directions, R is the proton range, y is the projection of R in a plane perpendicular to the neutron direction, b is the projection of y in a plane perpendicular to the emulsion surface and containing the proton track, and d is the emulsion thickness.

We now derive the probability p that a proton recoil produced by a neutron of energy E_n leaves the emulsion plate. For a given b, this is b/d. For a given value of y, we average b over all angles ψ (Fig. 4) to obtain

$$\frac{\int_0^{\pi/2} b(\psi)\,d\psi}{d \times \int_0^{\pi/2} d\psi} = \frac{2y}{\pi d} \tag{22}$$

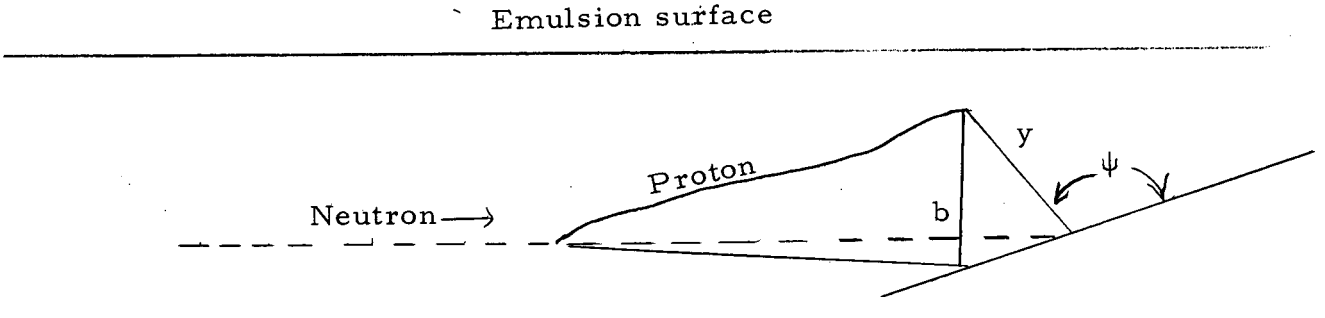

To go farther, we need a form for the range-energy relation for protons in emulsion. We use the relation $R = (E/A)^{\gamma}$, with $A = 0.22$ and $\gamma = 1.67$.[27] We can then write

$$b = R \sin\theta = \left(\frac{E}{A}\right)^{\gamma} \sin\theta, \tag{23}$$

where E, the energy of the proton, is given by $E = E_n \cos^2\theta$. Combining this relation with Eqs. (22) and (23), we have, for P as a function of E_n and θ,

$$P(\theta, E_n) = \frac{2}{\pi d} \left(\frac{E_n}{A}\right)^{\gamma} (\cos\theta)^{2\gamma} \sin\theta.$$

Finally, to obtain P as a function of only the neutron energy, we need to integrate over the distribution of scattering angles $f(\theta)$. This is

$$f(\theta) + \frac{2 \sin 2\theta}{1 - \cos^2\theta_{max}} ,$$

where θ_{max} is the half angle of the acceptance cone for recoil protons. Then we have

$$P(E_n) = \int_0^{\theta_{max}} P(\theta, E_n) f(\theta) d\theta$$

$$= \frac{8\left(\frac{E_n}{A}\right)^{\gamma}}{\pi d(1-\cos^2\theta_{max})} \int_0^{\theta_{max}} (\cos\theta^{2\gamma+1} - \cos\theta^{2\gamma+3}) d\theta = \frac{R_{max}}{d} J(\theta_{max}),$$

where R_{max} is $\left(\frac{E_n}{A}\right)^{\gamma}$, and

$$J(\theta_{max}) = \frac{8}{\pi(1-\cos^2\theta_{max})} \int_0^{\theta_{max}} (\cos\theta^{2\gamma+1} - \cos\theta^{2\gamma+3}) d\theta. \tag{24}$$

Values of $J(\theta_{max})$ were tabulated numerically and are shown in Fig. 25. It is to be noted that these formulae are valid only for energies, such that the maximum value of y is less than the emulsion thickness d. By differentiating $P(\theta, E_n)$, it is found that the maximum transverse range y_{max} occurs when $\theta = 29$ deg. If we then require that y_{max} be less than 600 μ, we find that the highest-energy neutrons for which the calculation holds is 20 MeV.

b. Corrections for multiple scattering

For a track that undergoes scattering, the vertical extent of the track b' exceeds the analogous quantity b for a "geometric track" by an amount we call $\Delta b'$. Let α be the dip angle of the track; for $\alpha = 0$, $\Delta b'$ is simply

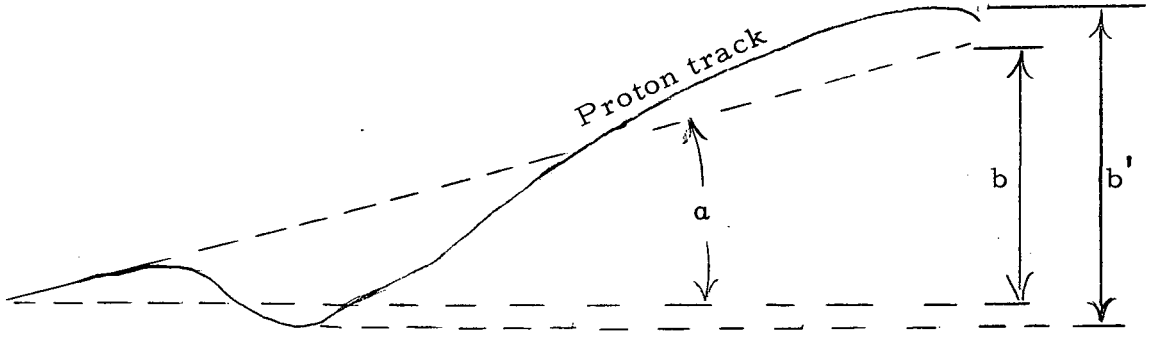

the transverse range y and is thus positive. As α increases, $\Delta b'$ decreases rapidly, and finally, for large dip angles, actually becomes negative. This is evident, for when $\alpha = 90$ deg, then $\Delta b'$ becomes $R_p - R$. The quantity $\Delta b'$ was measured for values of α other than 0 deg by drawing replicas of the tracks on graph paper and taking appropriate measurements from the drawings. For short tracks (<1 mm), direct measurements of $\Delta b'$ were made with use of an eyepiece reticle. The results are shown as circles on Fig. 26. The lines were arbitrarily

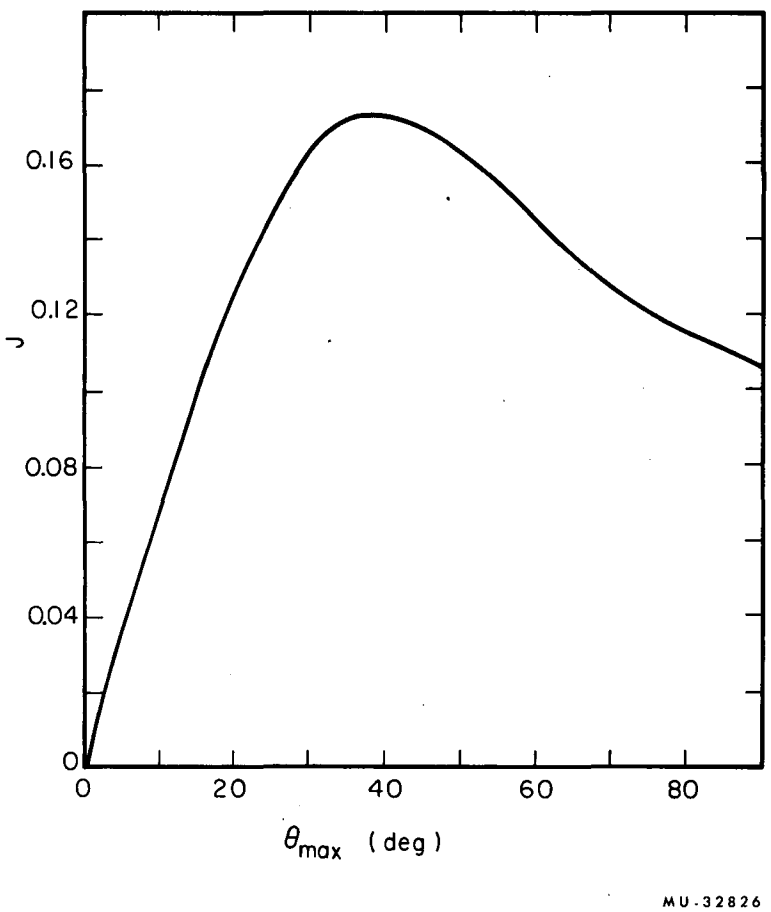

Fig. 25. Values of the integral $J(\theta_{max})$. The escape probability is given by

$$P(E_n) = \frac{R_{max}(E_n)}{d} J(\theta_{max}).$$

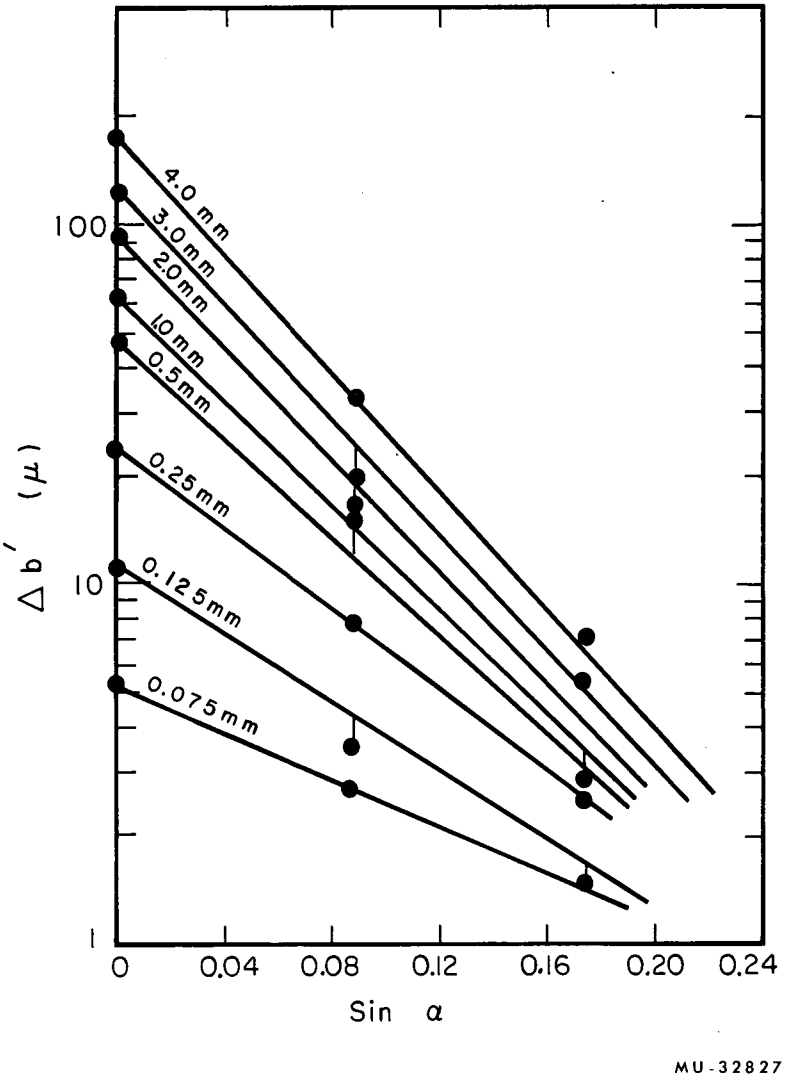

Fig. 26. $\Delta b'$ vs sin α. The intercepts at sin $\alpha = 0$ are well measured, but the slopes are roughly interpolated from a few scattered data points.

drawn to fit the data and to make $\Delta b'$ a smooth function of $\sin\alpha$ and the range. This graph was then used to determine the corrections to the escape probability. The corrected escape probability now becomes

$$P'(\theta_{max}E) = \int_0^{\theta_{max}} d\theta \int_0^{\pi/2} d\psi \frac{b'(\theta,\psi)}{d} f(\theta)f(\psi)$$

$$= P(\theta_{max}, E) + \int_0^{\theta_{max}} d\theta \int_0^{\pi/2} d\psi \frac{\Delta b'(\theta,\psi)}{d} f(\theta)f(\psi),$$

where $f(\theta)$ and $f(\psi)$ are properly normalized distribution functions for θ and ψ. The integral can be done in a straightforward way, for if θ, ψ, and E are given, then the proton range and dip angle α can be calculated. Then $\Delta b'$ can be obtained from Fig. 26. The values of the escape probability P, calculated in the straight-track approximation, and with corrections for multiple scattering, are shown in Figs. 27 to 30.

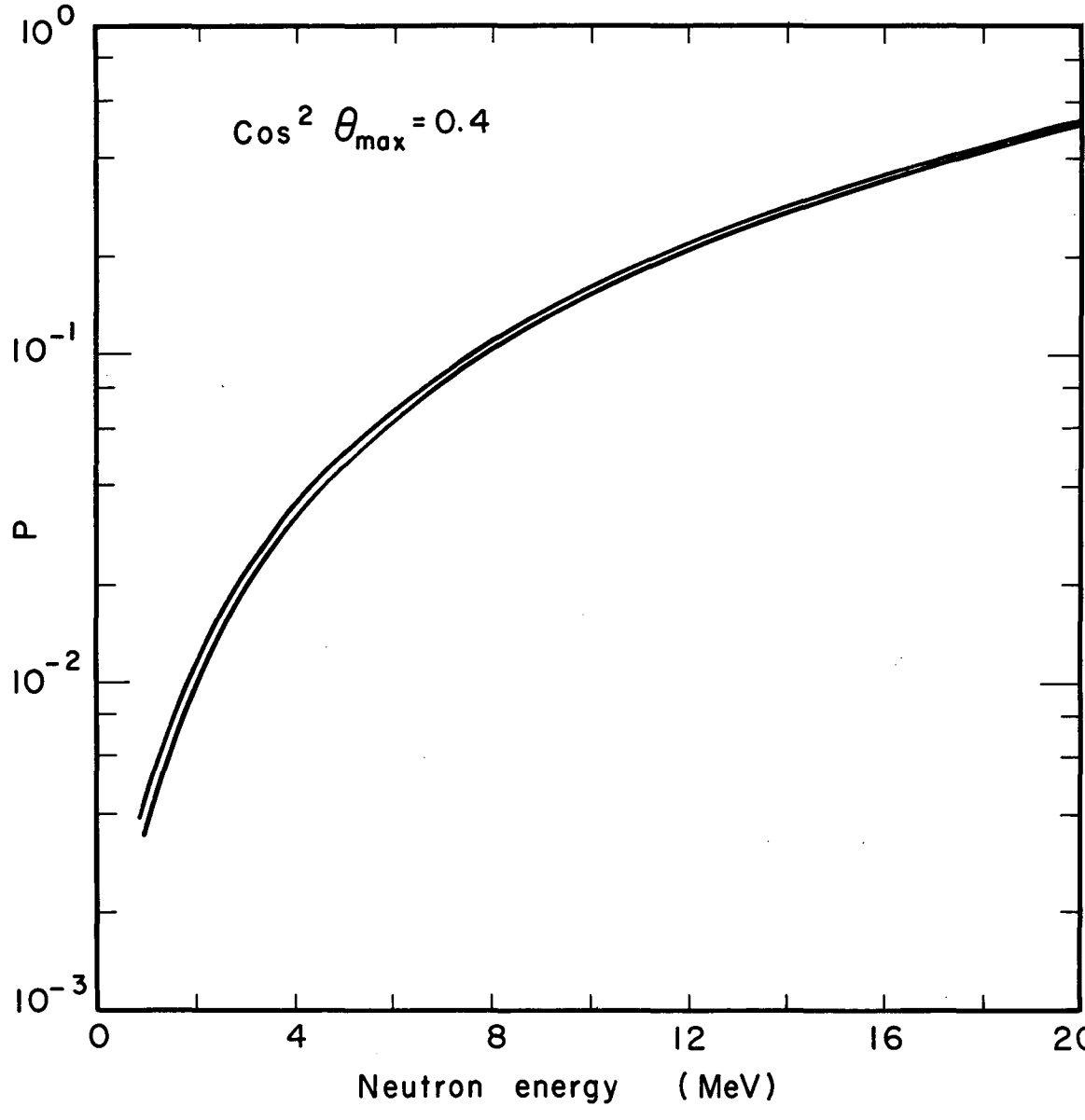

Fig. 27. The escape probability P vs neutron energy. The lower curve is without corrections for multiple scattering. The upper curve includes these corrections.

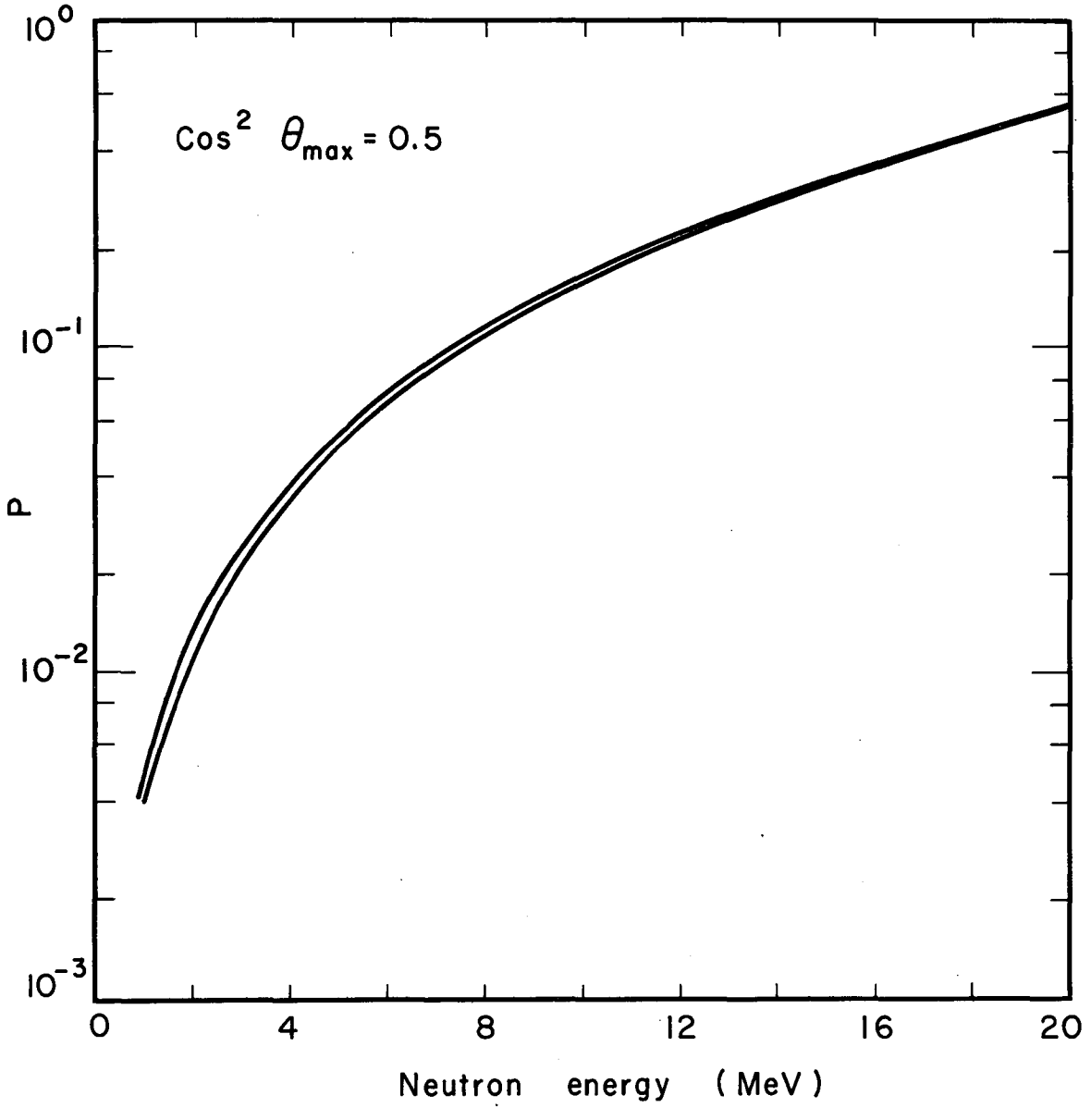

Fig. 28. The escape probability P vs neutron energy. The lower curve is without corrections for multiple scattering. The upper curve includes these corrections.

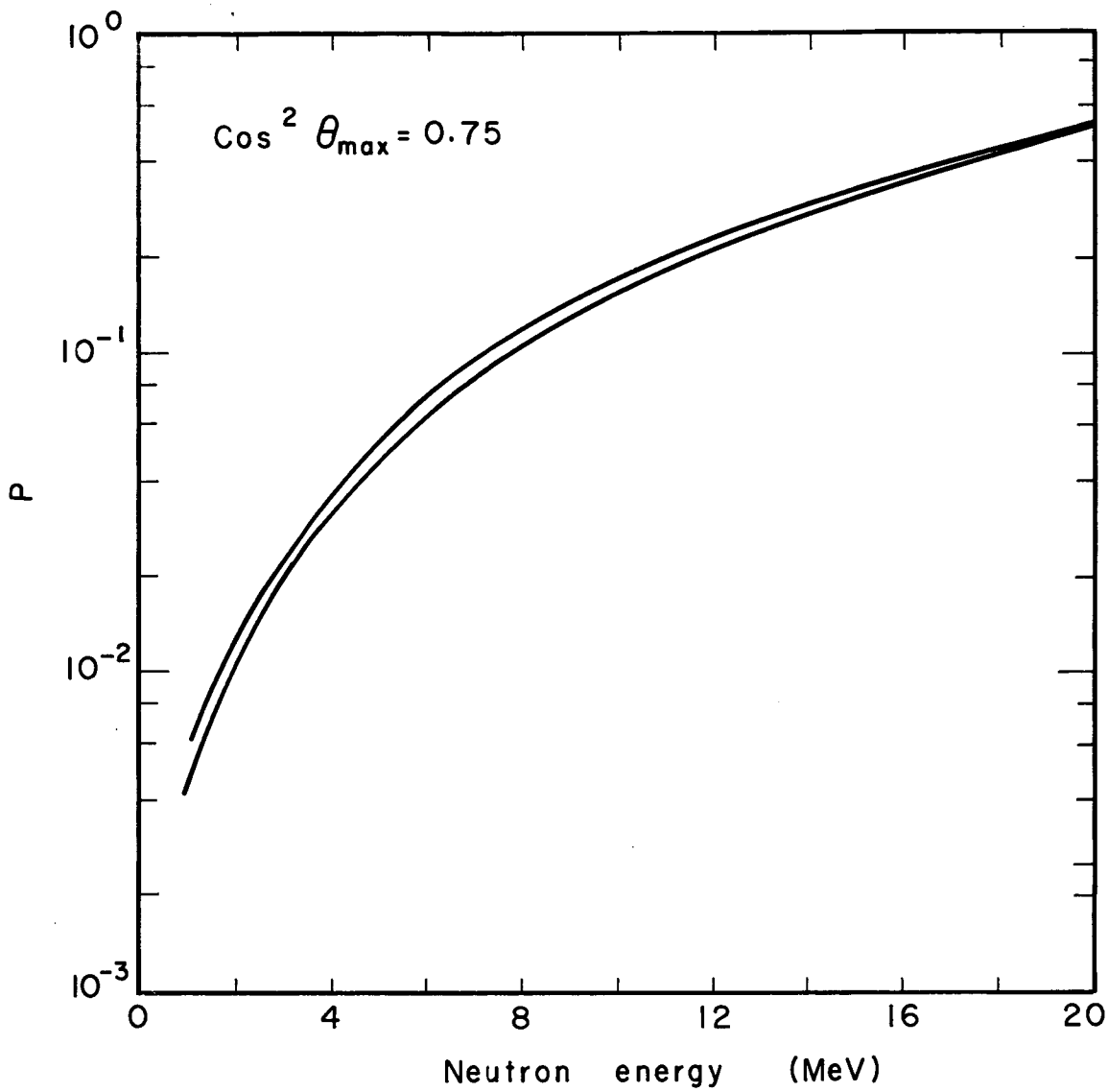

MUB-2270

Fig. 29. The escape probability P vs neutron energy. The lower curve is without corrections for multiple scattering. The upper curve includes these corrections.

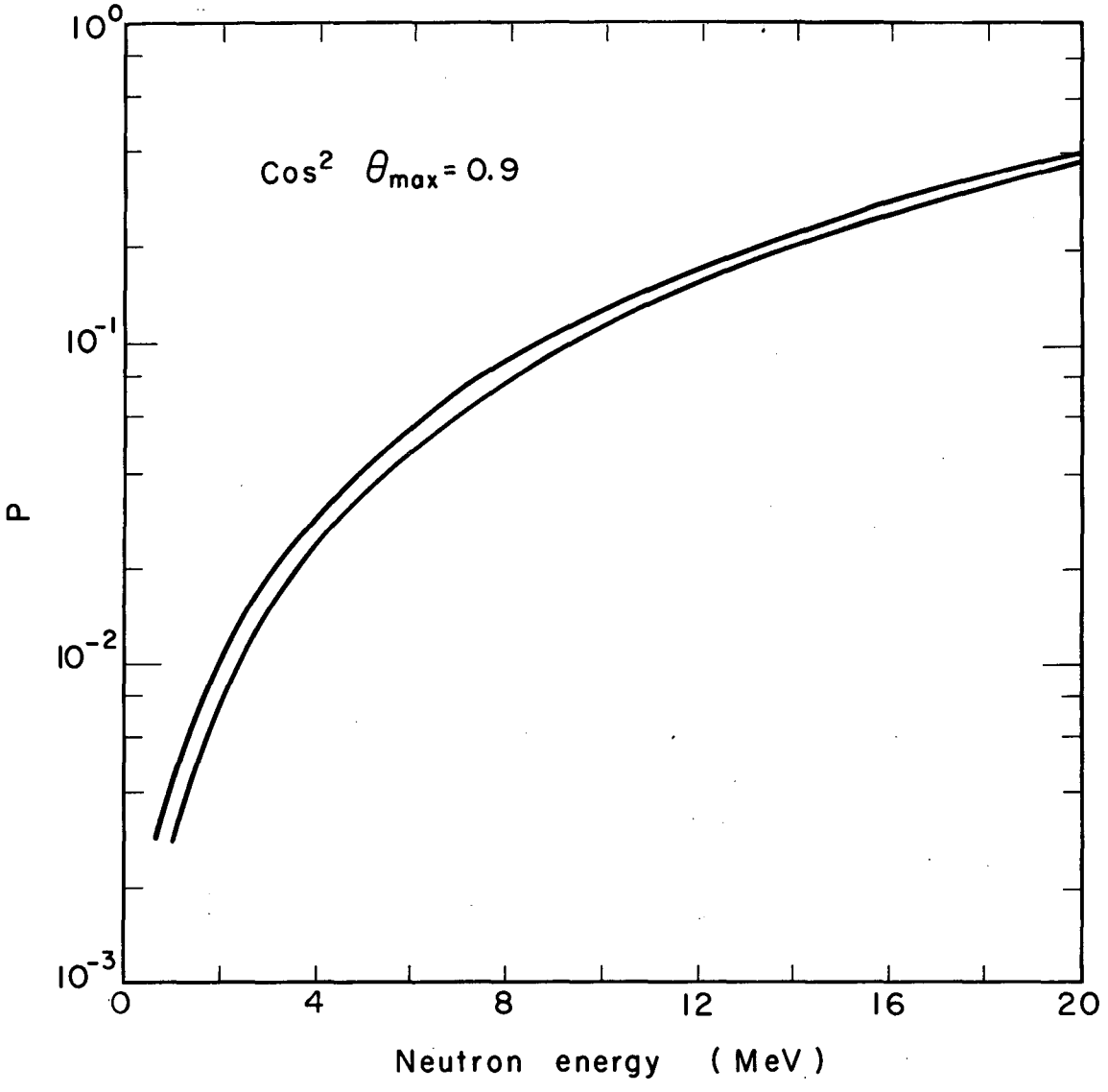

Fig. 30. The escape probability P vs neutron energy. The lower curve is without corrections for multiple scattering. The upper curve includes these corrections.

APPENDIX III

A. Calculation of the Angular Distributions of Neutrons Evaporated from Fission Fragments

We assume the rather general form

$$\frac{d^2\sigma}{d\Omega dE} \propto E_F^n \exp(-E_F/T)\,(1+a\cos^2\theta_F)$$

for the neutron spectrum in the moving fragment center-of-mass frame. Here,

E_F is the neutron energy in the fragment system,

$\cos\theta_F$ is the angle of emission of the neutron with respect to the fragment direction,

and T is the nuclear temperature of the fragment; n and a are adjustable parameters.

For $n=1$ and $a=0$, we have a Weisskopf distribution; for $n=1/2$ and $a=0$, we have a Maxwell distribution.

Three reference frames are used in these calculations. These are illustrated in Fig. 31. The F frame moves with the fragment and has the fragment direction as its z axis. The C frame moves with the c. m. of the compound nucleus and has its z axis in the direction of motion of the fragment. The O frame moves with the compound-nucleus system and has its z axis in the beam direction. The plane, defined by ψ (the azimuthal angle) equals zero, is the same for all three frames. The subscripts F, c, and o are used to define the reference frame, and the symbols used are

E = neutron energy,

τ = energy per neutron mass of fission fragment in the compound nucleus system,

θ = polar angle,

ψ = azimuthal angle,

and α = angle between the beam direction and the fragment direction in the compound-nucleus system.

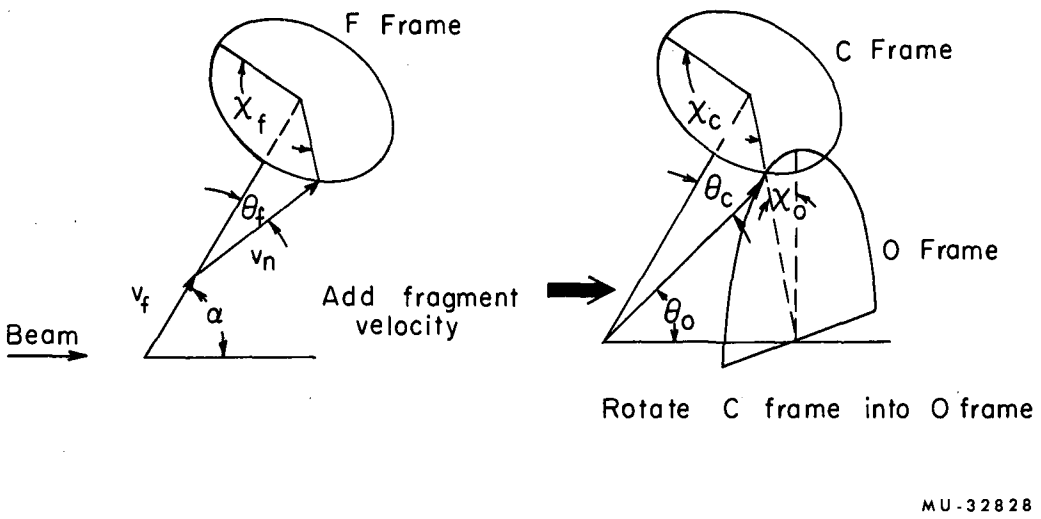

Fig. 31. Reference frames used in the calculations of Appendix III.

The cross section in the c system is then

$$\frac{d^2\sigma_c}{d\Omega_c dE_c} = \left(\frac{E_c}{E_F}\right)^{1/2} \frac{d^2\sigma_F}{d\Omega_F dE_F} \quad .$$

Using the relations

$$E_F = E_c + \tau - 2(E_c\tau)^{1/2}\cos\theta_c$$

and

$$\sin\theta_F = \sin\theta_c \left(\frac{E_c}{E_F}\right)^{1/2} ,$$

one obtains

$$\left.\frac{d^2\sigma}{d\Omega_c dE_c}\right|_{1F} \propto (E_c)^{1/2}[E_c + \tau - 2(E_c\tau)^{1/2}\cos\theta_c]^{n-1/2}$$

$$\times \exp\{-[E_c + \tau - 2(E_c\tau)^{1/2}\cos\theta]/\tau\}$$

$$\times \left\{1 + a\left[1 - \frac{E_c}{E_c + \tau - 2(E_c\tau)^{1/2}\cos\theta_c}\sin^2\theta_c\right]\right\}.$$

The subscript 1F indicates that evaporation from only a single fragment has been considered. The distribution in the compound system with the z axis along the beam direction must now be considered. This requires only a rotation, so that energy variables are not affected ($E_c = E_o$, etc.). The angle θ_c must be expressed in terms of O coordinates. A vector (Fig. 30) with coordinates θ_o, ψ_o has projection on the z axis equal to $\cos\alpha\cos\theta_o + \sin\alpha\sin\theta_o\cos\psi_o$, and hence this values of $\cos\theta_c$. Using this relation, we obtain for the distribution in the O frame

$$\frac{d^2\sigma}{d\Omega_c dE_o} = E_o^{1/2} x^{n-1/2} e^{-x/\tau}\left[1 + a\left(1 - \frac{E_c}{x}Q^2\right)\right] , \qquad (4)$$

where $x = E_o + \tau - 2Q(E_o\tau)^{1/2}$, and $Q = \sin\theta_o \sin a \cos\psi + \cos a \cos\theta_o$. An integration over the fission-fragment distribution still remains. Because of the azimuthal symmetry, an integration over ψ_o is equivalent to an integration over the azimuthal angle of the fragment distribution. Let the fragment distribution be $W_f(a)da$. The neutron distribution from a distribution of fragments becomes

$$\frac{d^2\sigma}{d\Omega_o dE_o} \propto \int_{\psi=0}^{\pi} d\psi \int_{\theta=0}^{\pi} da\, dE_o^{1/2} x^{n-1/2} e^{-x/\tau}\left[1+a\left(1-\frac{E_c}{x}Q^2\right)\right]$$

$$\times W(a)\sin a. \qquad (5)$$

Equation (5) was integrated numerically with the aid of an IBM 7090 computer for several representative combinations of values of the parameters T, a, and n. Temperatures of 1.5 and 2 MeV were used. Values of n used were 1 (Weisskopf distribution) and 1/2 (Maxwell distribution).

Values of the anisotropy coefficient a of 0 and 0.5 were used. The fragment velocity per neutron mass is 0.72 MeV.[30] The empirical curve

$$W(a) \propto \left(\frac{1.0917}{\sin^2 a + 0.0917}\right)^{0.6}$$

was found to fit well the results of Viola's measurements of the fission-keep fragment angular distribution[5] and was used in these calculations.

ACKNOWLEDGMENTS

I am especially grateful to Dr. Walter H. Barkas for suggesting this work and for his continued guidance. I am grateful to Dr. Robert L. Thornton and Dr. David L. Judd for their interest and encouragement.

I am deeply grateful to my wife Frances, who wrote some of the computer programs in addition to giving invaluable moral support and encouragement.

I wish to thank those people who did the emulsion scanning: Mr. Ridgway Banks, Miss Olga Fekula, Mr. John Paul, and Mr. Gary Williams.

I appreciate the many helpful discussions and suggestions from Dr. Harry Heckman, Mr. Donald Reames, and Miss Frances Smith.

I owe my appreciation to Dr. Edward Hubbard and the Hilac crew for their help in running the experiment, to Mr. Carl Cole who processed the emulsions, and to Dr. Stanley Cohen, Dr. Wladyslaw Swiatecki, and Mr. Franz Plasil for making available the results of their calculations before publication.

This work was done under the auspices of the U. S. Atomic Energy Commission.

REFERENCES

1. H. C. Britt and A. R. Quinton, Phys. Rev. 124, 877 (1961).
2. T. Ericson, Advances in Physics, 9, 425 (1960).
3. H. C. Britt and A. R. Quinton, Reactions Between Complex Nuclei (John Wiley and Sons, Inc., New York, N. Y., 1960).
4. D. V. Reames, Emission of Charged Particles in Heavy-Ion Reactions, Lawrence Radiation Laboratory Report UCRL-10693, April 12, 1963 (unpublished), to be published by University of California Press, Berkeley, California.
5. Victor E. Viola, Jr., Angular Distributions From Heavy-Ion-induced Fission, (Thesis), Lawrence Radiation Laboratory Report UCRL-9610, March 24, 1961 (unpublished).
6. H. Marshall Blann, Fission of Gold With 112-MeV C^{12} Ions: A Yield-Mass and Charge-Distribution Study, (Thesis), Lawrence Radiation Laboratory Report UCRL-9190, 1960 (unpublished).
7. T. D. Thomas, G. E. Gordon, R. Latimer, and G. T. Seaborg, Phys. Rev. 126, 1805 (1962).
8. E. L. Hubbard, R. M. Main, and R. V. Pyle, Phys. Rev. 125, 1350 (1962).
9. H. W. Brock, Phys. Rev. 124, 233 (1961).
10. H. H. Heckman, B. L. Perkins, W. G. Simon, W. H. Barkas, and F. M. Smith, Phys. Rev. 117, 554 (1960).
11. Walter H. Barkas, Nuclear Research Emulsions, Vol. 1 (Academic Press, New York and London 1963), Chap. 9.
12. L. C. Northcliffe, Phys. Rev. 120, 1744 (1960).
13. Walter H. Barkas, Nuclear Research Emulsions, Vol. 1. (Academic Press, New York and London 1963), Chap. 10.
14. Louis Rosen, Nucleonics, Vol. 11, No. 8, p. 38 (1953).
15. J. B. Marion and J. L. Fowler, Editors, Fast Neutron Physics, Vol. II, (Interscience Publishers, Inc., New York, to be published).
16. John Gilmore, The Effects of Angular Momentum on Fission Probability, Lawrence Radiation Laboratory Report UCRL-9304, July 1960 (unpublished).

17. T. Sikkeland, E. L. Haines, and V. E. Viola, Jr., Phys. Rev. 125, 1350 (1962).
18. P. L. Allen, Nucl. Phys. 10, 348 (1959).
19. A. C. Douglas and N. MacDonald, Nuclear Phys. 13, 382 (1959).
20. K. J. Le Couteur, Proc. Phys. Soc. (London), A 65, 718 (1952).
21. T. D. Thomas, Phys. Rev. 116, 703 (1959).
22. J. R. Huizenga and R. Vandenbosch, Nuclear Reactions, Vol. 2, edited by P. M. Endt and P. B. Smith (Interscience Publishers, Inc., New York, 1962).
23. R. Vandenbosch, H. Warhanck, and J. R. Huizenga, Phys. Rev. 124, 847 (1961).
24. A. G. W. Cameron, Chalk River Project Report CRP-690, March 1957 (unpublished).
25. S. Cohen (Argonne National Laboratory) and F. Plasil and W. J. Swiatecki (Lawrence Radiation Laboratory), private communication.
26. N. A. Perfilov, O. V. Lozhkin, and V. I. Ostrounov, Nuclear Reactions Induced by High Energy Particles (Acad. Sci. USSR), UCRL-Trans-949 by Sergey Shewchuck.
27. Walter H. Barkas, Nuclear Research Emulsions, Vol. I (Academic Press, New York and London 1963), Chap. 8 and 10.
28. G. Molière, Z. Naturforsch 3a, 78 (1948).
29. Hans A. Bethe, Phys. Rev. 89, 1256 (1952).
30. H. C. Britt and A. R. Quinton, Phys. Rev. 120, 1768 (1960).
31. James C. Hodges, Microscope Equipment for Nuclear-Emulsion Analysis, Lawrence Radiation Laboratory Report UCRL-9089, 1960 (unpublished).